DESIGN AND FABRICATION OF OPTICAL FILTERS FOR LONG WAVELENGTH SPECTROSCOPY APPLICATION

by

Ayman Mohamad Zohbi

A dissertation submitted to the faculty of
The University of North Carolina at Charlotte
In partial fulfillment of the requirements
for the degree of Doctor of Philosophy in
Electrical Engineering

Charlotte

2012

Approved by:

____
Dr. Mohamad-Ali Hasan

____
Dr. Farid Tranjan

____
Dr. Stephen Bobbio

____
Dr. Yildirim Aktas

ABSTRACT

AYMAN MOHAMAD ZOHBI. Design and fabrication of thin-film optical filters for long wavelengths spectroscopy application. (Under the direction of Dr. MOHAMAD-ALI HASAN).

The design and fabrication of thin film Fabry-Perot interferometer (FPI) for long wavelength spectroscopy application is demonstrated. The system is designed to be integrated in a small portable spectrometer for the measurement of molecular absorption or emission as well as substance that has an infrared signature.

A Fabry-Perot interferometer with dielectric mirrors was fabricated using fabrication process on a silicon substrate. The FPI was made of multi thin layers, deposited on silicon (Si) substrate, alternating between high and low refractive-index (n) layers. Si was used as a substrate due to the high precision of etching achievable using conventional VLSI fabrication techniques. Since the wavelength of interest was in the far infrared (5 to 15 micrometers), the layers were selected carefully to minimize the thickness required to meet the quarter-wave optical-thickness criteria for the interferometer. Another criterion that had to be met is the ratio of the refractive indices (n) between the layers. In this study, we have utilized germanium (Ge), which has n value of ~ 4 in the wavelength range of interest, and zinc oxide (ZnO), which has n value average of ~1.8 in the range of interest. Deposition of the layers was carried out using electron beam deposition for Ge and sputtering for ZnO. First the Si substrate was etched precisely to provide the gap needed for the wavelengths on interest and then the dielectric layers were deposited. For example, using Ge thickness of 0.576 µm, ZnO thickness of 1.22 µm, and a gap of 4.77 µm, we have demonstrated a filter transmitting a wavelength of 9.2 micrometers with a full width at half maximum of ~ 0.5 microns using one stack of Ge/ZnO layers. Simulations, using Freesnell software, were consistent with the experimental results.

The tuning of the FPI with different cavity distances was demonstrated by measuring the transmission spectrum of the FPI. The transmission measurement was carried out using Fourier Transform Infrared Spectroscopy (FTIR) while the thickness of the layers was confirmed by scanning electron microscopy (SEM).

ACKNOWLEDGEMENT

I would like to express my deep and sincere gratitude to my advisor Dr. Mohamad-Ali Hasan for his endless support, encouragement, and motivation during this journey.

I am deeply grateful to my committee members, Dr. Farid Tranjan, Dr. Stephen Bobbio, and Dr. Yildirim Aktas for their kind support and excellent advice.

My sincere thanks are due to Dr. Muhammad Hashmi for his valuable guidance and friendly help.

I am grateful for the Electrical Engineering department at UNCCharlotte and all the professors who taught me and guided me during my time at UNCC.

I owe my loving thanks to my wife and my parents for their endless trust and encouragement.

And last but not least I owe a big thank you to my brother-in-law Firas for his help and support without which this accomplishment wouldn’t have been possible.

TABLE OF CONTENTS

LIST OF FIGURES

CHAPTER I: INTRODUCTION

Optical thin film filters are essential components in blocking or transmitting specific wavelengths and they are used in a wide variety of applications and industries. For instance they are used in telecommunication networks, in astronomy, in gravitational wave detection, in gas detection, in medicine spectroscopy, etc.

Infrared spectroscopy has long been used in the medical field for non-invasive measurement in many areas ranging from the amount of oxygen in the blood to optical tomography [13, 14].

One very promising usage of spectroscopy is the measuring of blood glucose level for diabetic patients.

Glucose is a monosaccharide sugar and it belongs to the carbohydrates family. The glucose molecule contains 6 Carbon atoms, 12 Hydrogen atoms, and 6 Oxygen atoms $C_6H_{12}O_6$. It is the main source of energy for the human body; however when the body cannot maintain the glucose level within 65-100 mg/mL, diabetes is developed [15].

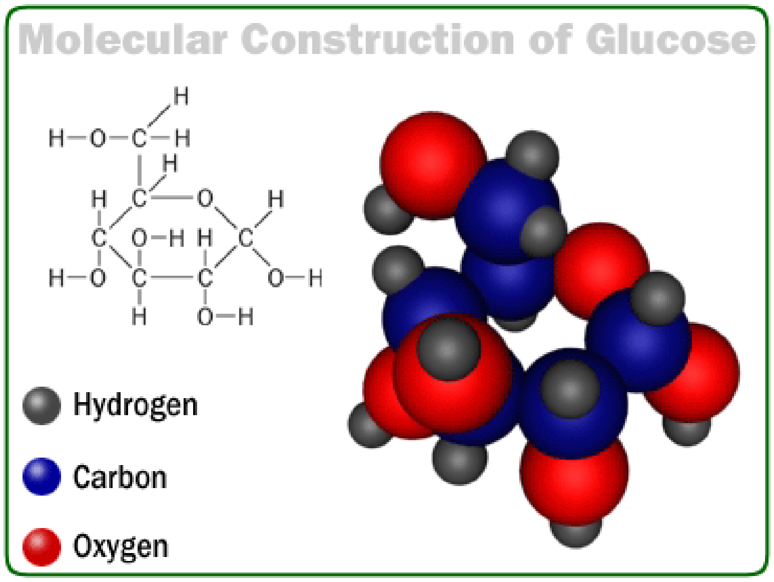

Figure 1.1: Glucose molecule structure [16].

The body regulates the glucose level by the means of insulin. Insulin is a hormone produced in the Islets of Langerhans in the beta cells of the pancreas; it interacts with the insulin receptor in the cells to open the glucose channels and consequently allows the glucose to transfer from the blood stream into cells and tissues [17,18].

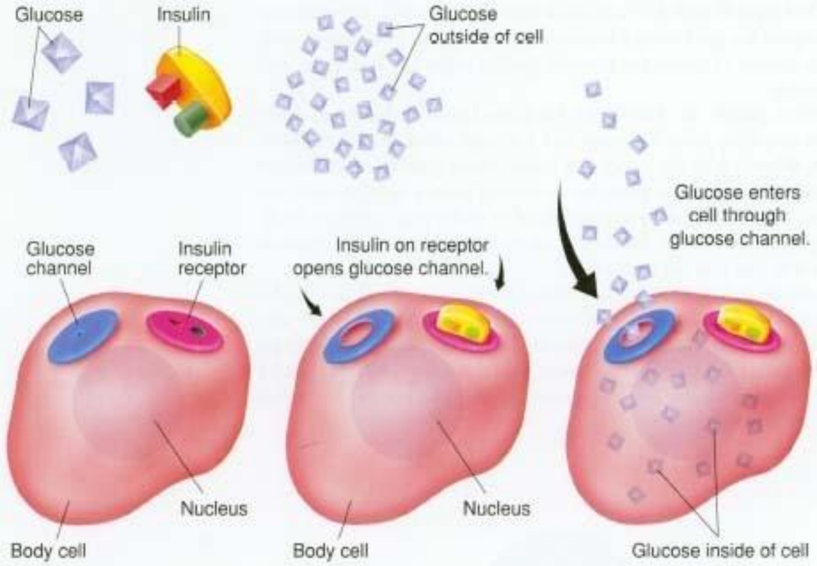

Figure 1.2: The process of glucose transfer to cells [17].

Diabetes is one of the major health issues in the world because of its total number of patients, cost, and mortality. According to the International Diabetes Federation (IDF) diabetes has an estimated 366 million patients worldwide and an estimated healthcare cost reaching $465 billion per year and it is blamed for 4.6 million deaths in 2011 [9].

In the United Sates alone, according to the Centers for Disease Control and Prevention (CDC), about 25.8 million patients , or 8.3 % of U.S population, suffered from diabetes in 2011, the healthcare cost reaches $174 billion annually and the projected number of patients will increase to 1 in 3 Americans by 2050 [8].

The Centers for Disease Control and Prevention (CDC) estimates that only 18.8 million patients are diagnosed and the remaining 7 million patients or 27% of diabetics do not know they have the disease [3].

There are two main types of diabetes, type 1 which is characterized by the pancreas' failure to produce insulin in the body, and type 2, less serious, which is characterized by the pancreas' failure to produce enough insulin in the body [1, 2].

The severity of diabetes is not in the disease itself only but in the chronic complications that are associated with it, such as heart disease and stroke, high blood pressure, blindness, amputations, nervous system disease etc.

Therefore a reliable technology that enables people to monitor and control diabetes has become an urgent necessity.

The effort to develop a continuous glucose monitoring system goes back to the year 1965 when Kadish and Hall who designed a system to continuously monitor the glucose level by measuring the amount of dissolved oxygen in the blood [4].

Over the years and due to the growing need for a continuous glucose monitoring system many measurement methods have been developed to meet this objective and they are presented below [5, 6, 10, 11]:

1.1 Glucose Sensing Methods

1.1.1 Minimum-invasive sensors

1.1.1.1 Needle/flexible wire amperometric enzyme electrode

This method is based on the glucose oxidase enzyme. The enzyme is fixated on a charged electrode at the tip of the needle or the flexible wire. When the glucose oxidizes upon reacting with the enzyme, it releases an electrical current proportional to the glucose concentration. The chemical reaction happens according to equations 1.1 and 1.2 below:

$$\text{Glucose} + O_2 \xrightarrow{\text{glucose oxidase}} H_2O_2 + \text{gluconic acid} \quad \text{(eq. 1.1)}$$

$$H_2O_2 \xrightarrow{700\text{mV}} O_2 + 2e^- \quad \text{(eq. 1.2)}$$

The glucose reacts with the glucose oxidase to produce hydrogen peroxide (H_2O_2), which then in the presence of 700 mv potential oxidizes at the electrode and generate electrons. The signal is then correlated to the glucose level.

Medtronic is the only company that uses this technology for continuous monitoring of glucose where a needle is inserted in the subcutaneous tissue.

Even though the sensor offers a continuous reading of glucose level, it however requires calibration and it suffers from a drift as compared to the actual sugar level in the blood and therefore it cannot be used in a closed-loop pancreas like system [10].

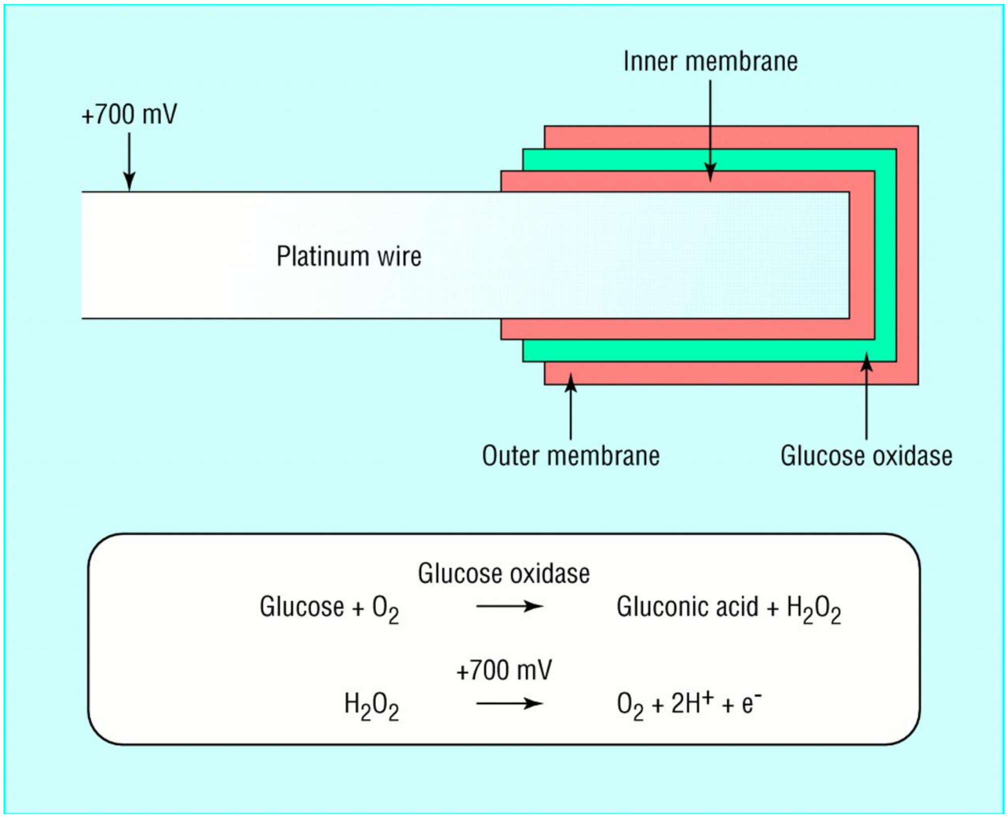

$$\text{Glucose} + O_2 \xrightarrow{\text{Glucose oxidase}} \text{Gluconic acid} + H_2O_2$$

$$H_2O_2 \xrightarrow{+700\ \text{mV}} O_2 + 2H^+ + e^-$$

Figure 1.3: Amperometric based sensor. Hydrogen peroxide produced by glucose oxidation is detected electrochemically [10].

1.1.1.2 Near-infrared fluorescence

In this method a fluorophore protein binds with the glucose. After binding to the glucose, the protein fluorescent characteristics change. This change is then detected by an external sensor.

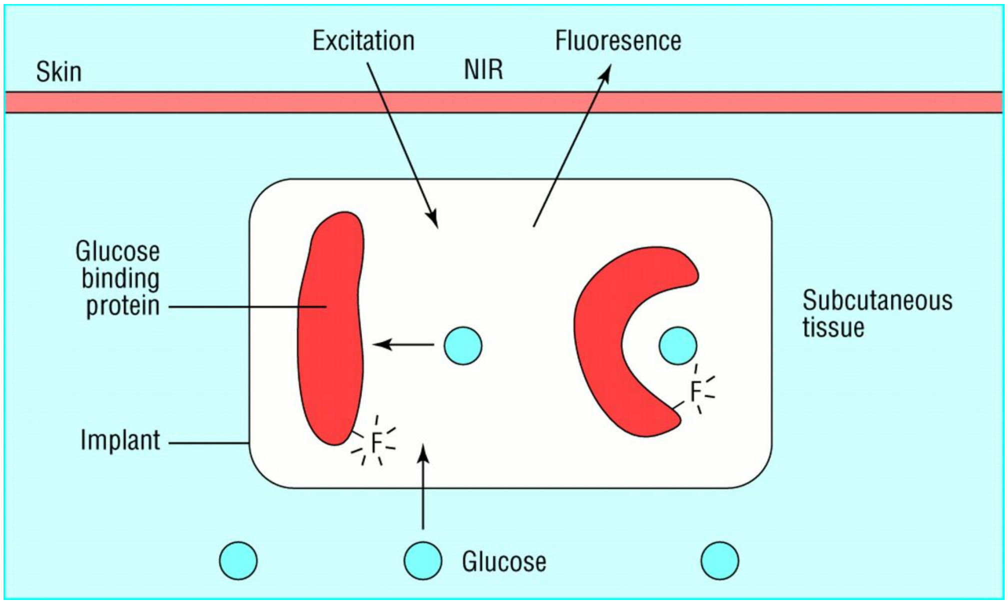

Figure 1.4: Glucose sensing with fluorophore (F) protein binding. Glucose binding changes the protein's fluorescent characteristics (increase or decrease, depending on the fluorophore) [10] .

1.1.1.3 Fluorescence-resonant-energy-transfer (FRET)

This sensor is based on the competitive binding of dextran, acceptor (A), to Concanavalin A, donor (D). A hollow dialysis fiber containing immobilized Concanavalin A to its inner wall is introduced to the tissue, the glucose molecules entering the tube disjoint the dextran from the bond and increase the distance between the acceptor and the donor, causing FRET to decrease and both fluorescence intensity and lifetime to increase. Then a sensor detects the fluorescence intensity and calculates the glucose level.

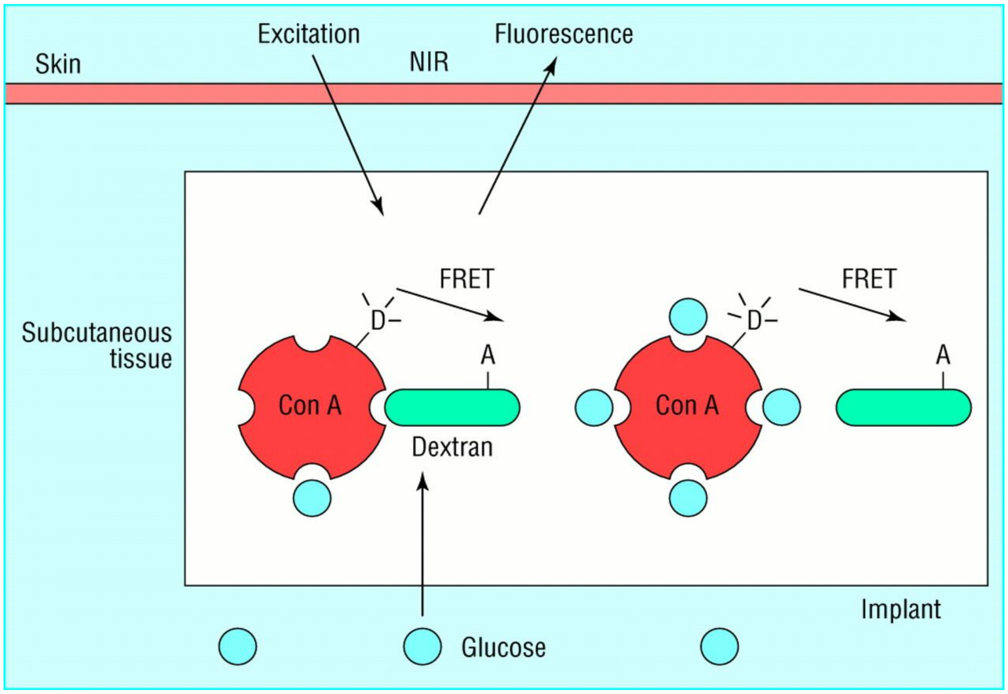

Figure 1.5: Glucose sensing with fluorescence resonance energy transfer (FRET).FRET occurs between Concanavalin A (Con A) and dextran. Displacement of dextran by glucose reduces FRET and increases fluorescence intensity and lifetime [10].

1.1.2 Micro-dialysis

1.1.2.1 Reverse iontophoresis

In this method a small current passed through the skin cause ions and glucose-containing interstitial fluid to move towards the skin surface where a glucose-oxidase based sensor measures the glucose level.

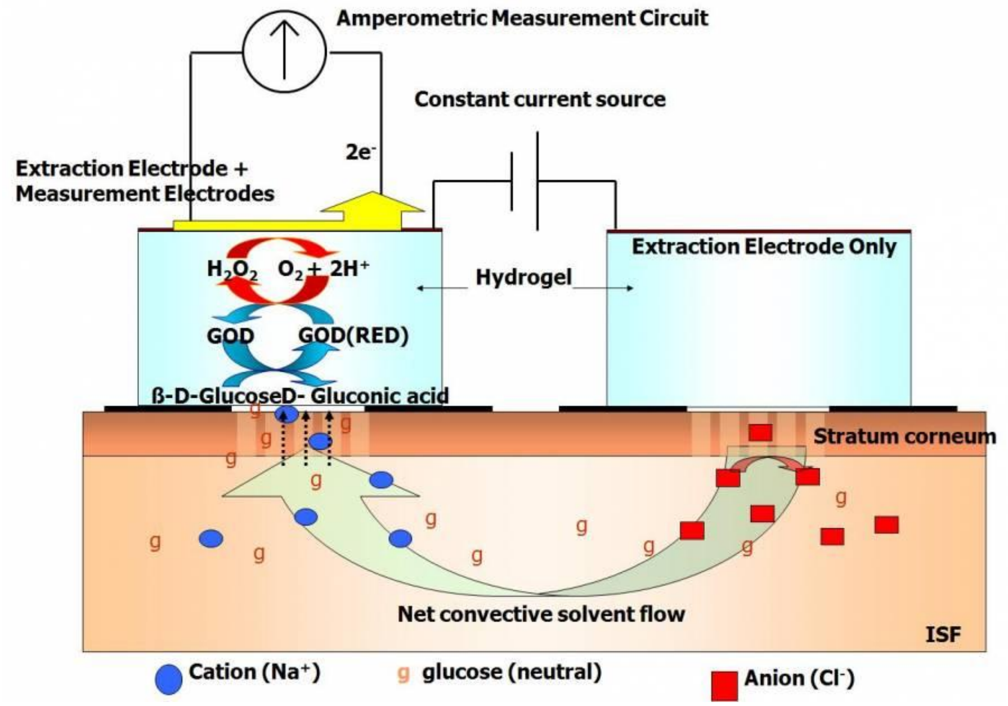

Figure 1.6: Transdermal glucose sensing where a current passing through the skin causes glucose-containing fluid to move to the surface of the skin where it is measured by amperometric sensor [11].

1.1.3 Non-invasive sensor

1.1.3.1 Mid-infrared spectroscopy

In this method a light is shined on the tissue, and the intensity of the light passing thru or reflected from the tissue is measured.

By adjusting the glucose spectra to a defined concentration of glucose, the glucose level can be obtained.

The infrared wavelengths of interest that have been reported in the literature as potential wavelengths for non-invasive measurement of glucose are in the range of 8 μm to 10 μm [7,85].

Although there are many research groups and companies working towards developing a non-invasive continuous glucose sensor, there is still no such a device in the current market.

In this dissertation, we propose in vitro and in vivo device to monitor glucose level using infrared absorption-signature of glucose.

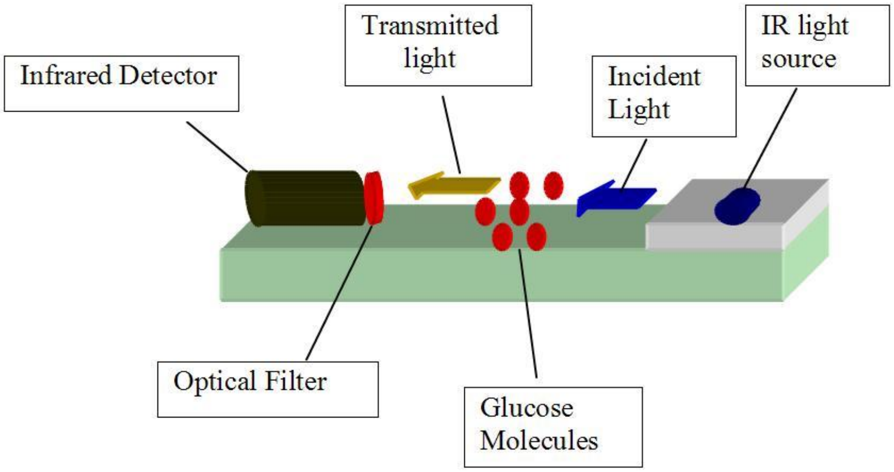

Figure 1.7: Conceptual drawing of the proposed infrared sensor. An infrared red source generating the incident light, after passing through the glucose molecules; the transmitted light is then filtered and measured. The light intensity will then be correlated to glucose concentration.

Figure 1.8 shows typical absorption spectra of glucose taken at various glucose concentration levels [7] while Figure 1.9 plots the changes in the components of peak 5 (in Fig. 1.8) with increasing glucose concentrations.

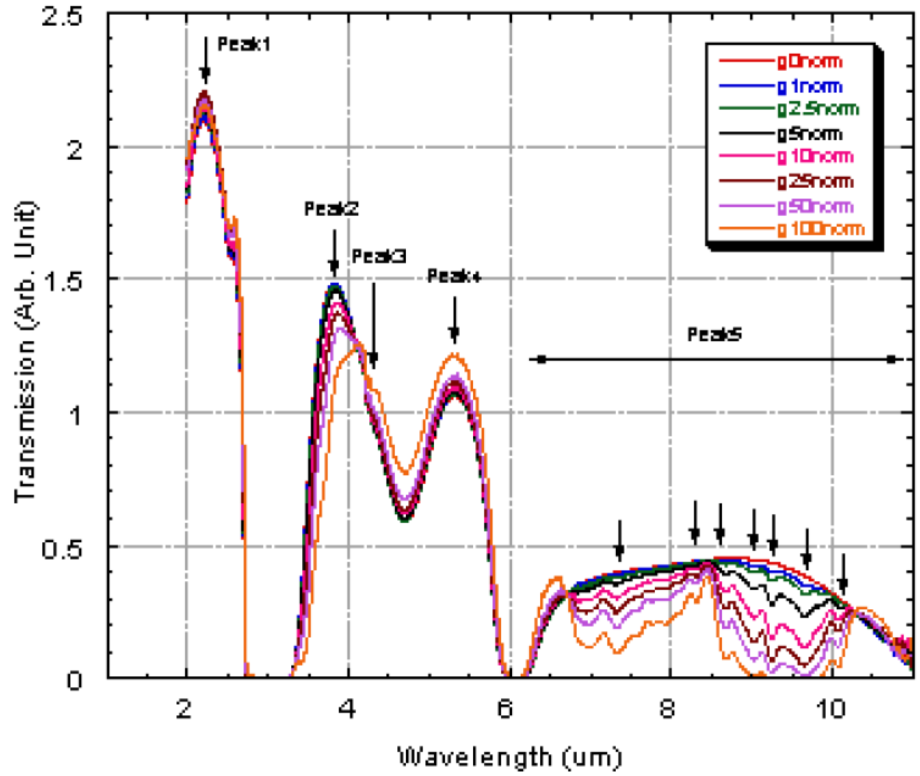

Figure 1.8: Transmission spectra of aqueous glucose solutions [7].

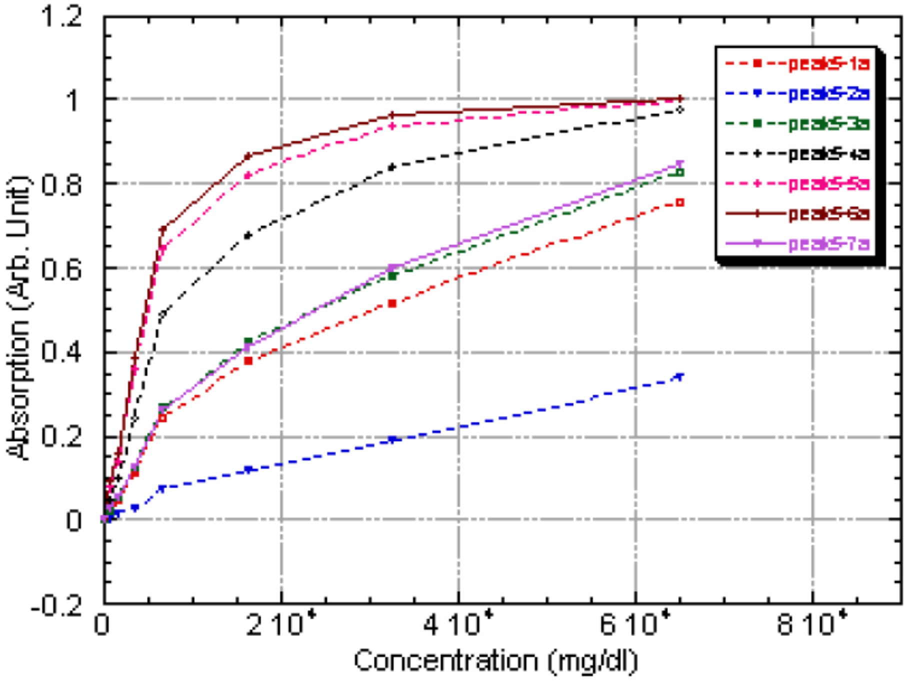

Figure 1.9: Change of selected Peak5 as function of glucose concentration [7].

While the absorption spectra are known, there are no simple, miniature detectors for this wavelength range. The proposed device is a miniature spectrometer that operates on the wavelengths of interest for measuring the glucose level.

A Typical IR Spectrometer consists of 3 main building blocks, an Infrared source, an interferometer or optical filter, and a detector.

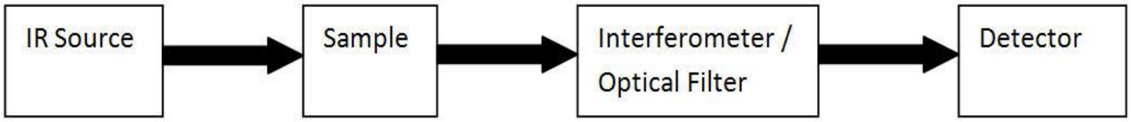

Figure 1.10: IR Spectrometer Block Diagram.

In the following chapters I will cover the existing and under development non-invasive glucose monitoring devices in the market, the different IR technology for sources and detectors and the design of an optical filter for the IR wavelengths.

CHAPTER II: EXISTING/UNDERDEVELOPMENT NON-INVASIVE GLUCOSE MONITORING DEVICES

2.1 Introduction

This chapter will shed the light on the current or under development non-invasive glucose monitoring devices, the technology they are using and the companies that are developing them.

There are two main technologies being largely investigated for the development of non-invasive glucose monitoring devices for the purpose of reducing the pain and discomfort associated with pricking the finger and testing blood.

1- Using the molecular properties of glucose such as infrared signature, optical rotation, Raman shifts, and photoacoustic absorption.

2- Looking at a correlation between the glucose level and its effect on the physical properties of blood and tissue, given that glucose is an important constituent of blood that influences the physicochemical parameters of the tissue.

There are many start-up companies working in developing new technologies and devices for noninvasive blood glucose monitoring. Some of the main companies that are involved in this field and their corresponding technologies are discussed below.

2.2 Eyesense

Eyesense is a startup company founded in 2006 as a spin-off from Novartis. The concept of Eyesense's glucose monitoring technology is based on the measurement of fluorescence of glucose in the interstitial fluid below the conjunctiva of the eye.

A mini chemical sensor is surgically inserted under the conjunctiva of the eye in a very short procedure. This sensor must be replaced annually by an ophthalmologist. The chemical sensor reacts with the blood glucose and sends a fluorescent light.

The fluorescent signal is then measured by an external small hand-held device, which correlates the glucose concentration to the light intensity and displays it on the screen. The device takes less than 20 seconds to finish the reading and the measurement can be taken as often as needed by the patient [86-87].

Eyesense is conducting large clinical trials to prove safety and effectiveness and plans to launch the product in 2013 [87].

2.3 Freedom Meditech

Freedom-Meditech is a US based start-up Company founded in December 2006. Freedom- Meditech has two non-invasive, ophthalmic medical devices currently under development. ClearPath DS-120 for the detection of chronic disease and the I-SugarX for diabetes management [86,88].

The I-SugarX glucose monitor detects glucose concentrations in the eye by shining a beam of light into the eye which is then measured, correlated to the glucose level, and then displayed on a handheld device [86,88].

The ClearPath DS-120 is intended as a non-invasive, in-office diabetes screening device for professionals. It works by scanning the eye with a low power blue light and the result is displayed at the point of care in less than 10 seconds. Its main objective is to identify patients who may be pre-diabetics or undiagnosed diabetics [86,88].

2.4 Calisto Medical

Calisto Medical is a US company that has been in operation since 2004 with the objective of becoming the leader in manufacturing and marketing non-invasive glucose monitoring devices. The company's main product is the Glucoband [86,89].

The Glucoband is a watch-like device that is worn on the wrist and uses Bio-Electromagnetic Resonance (BEMR) to continuously monitor glucose concentration. The BEMR concept is based on the fact that the electromagnetic molecular self-oscillation of glucose varies with the glucose concentrations, this phenomenon is referred to as glucose signatures. The Glucoband has a large database of glucose reference signatures covering the range of blood glucose concentration from 40mg/dl to 400mg/dl [86,89].

These reference signatures are matched against the self-oscillation waves in the human body to estimate the glucose levels. The device initial measurement can take few minutes, however in the monitoring mode; measurement can be continuous or intermittent with the frequency set by the user.

2.5 Diramed Technology

Diramed is a startup company whose technology is based on the concept of Raman Spectroscopy, which measures the intensity of the shifted scattered light. It utilizes a laser beam targeted at the patient's skin, upon impinging on the skin the light scatters. The scattered light is then captured by a detector, which measures the changes in the light frequency caused by the interaction between light and various constituents in the body.

Diramed device is initially intended to be used in hospitals and later on a smaller portable unit will be developed for home use [86,90].

2.6 Integrity Applications

Integrity Applications is an Israeli company founded in 2001. The company’s glucose monitoring device is called GlucoTrack. The device is designed to simultaneously yet independently measure the glucose concentration using three techniques, ultrasonic, electromagnetic, and thermal. Physically, the device consists of the main unit and an ear clip. The main unit contains the device electronics and signal processor and the ear clip comprises the three types of sensors needed for measurement [86,91].

The ear clip clips to the ear lobe and the three sensors collect the measurements simultaneously, the data is then send to the processor where it is analyzed correlated to the glucose concentration and then displayed on the LCD.

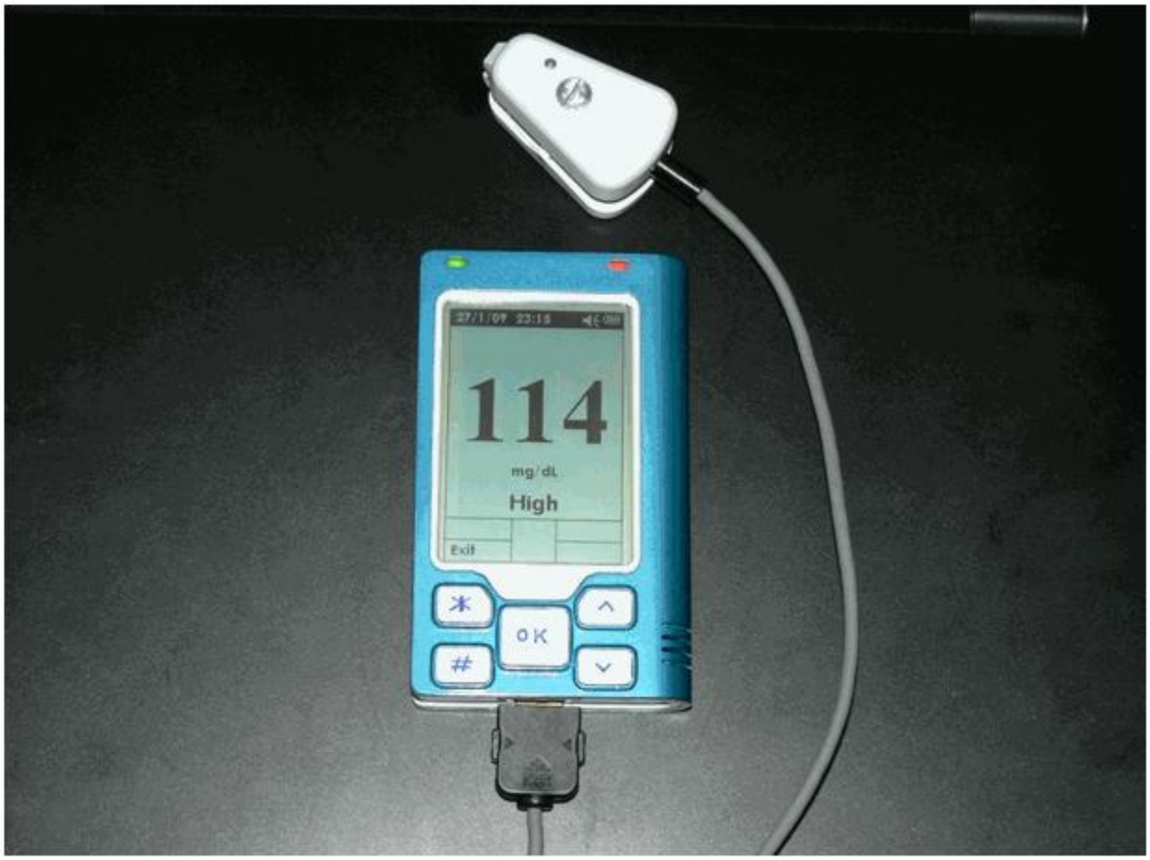

Figure 2.1: GlucoTrak glucose monitoring device [91].

2.7 Glucon

Glucon is an Israeli startup company founded in 2000. The company's main product is called Aprise and it uses photoacoustic technology to measure glucose concentration. The device uses a laser beam to generate acoustic signals in the vasculature. These acoustic signals are generated due to the absorption of light of a specific wavelength, which is influenced by glucose concentration. The optical properties of the tissue are then captured in an ultrasonic image, which resolves the blood vessel from the tissue layers around it. This gives an accurate picture of the glucose concentration in the blood [86].

Glucon is also working on a hospital based CGM device called Optimus. This device is intended to be attached to the existing vascular line attached to the patient. The device automatically draws blood at a fixed frequency by interrupting the intra-venous fluid line. The blood is then analyzed for glucose by the regular glucose oxidase lab method [86].

2.8 GlucoLight

GlucoLight was founded in 2003 and now it is out of business. The company developed a product called Sentris-100. The device utilizes an optical coherence tomography. The device consisted of a source for low coherence light, an interferometer with a reference arm and a sample arm, a moving mirror in the reference arm, and a photodetector to measure the transmitted signal. The amount of light scattered by the tissue depends on the refractive index of the interstitial fluid, which is proportional to the glucose concentration, and the refractive index of scattering centers such as constituents in the blood.

This scattered light by the tissue is combined with the light returned from the reference arm of the interferometer and the resulting signal is detected by a photodetector [86,94].

Figure 2.2: GlucoTrak glucose monitoring device [94].

2.9 Glumetrics

Glumetrics is a US based company whose main product is called GluCath. The Glucath is an intravenous continuous glucose monitor.

The device utilizes a proprietary fluorescent chemistry fixated at the tip of a miniature fiber optics. The fiber is inserted in a vein and the fluorescence is detected by blue light [86,92].

The product is intended to be used in the ICU environment for glycemic control.

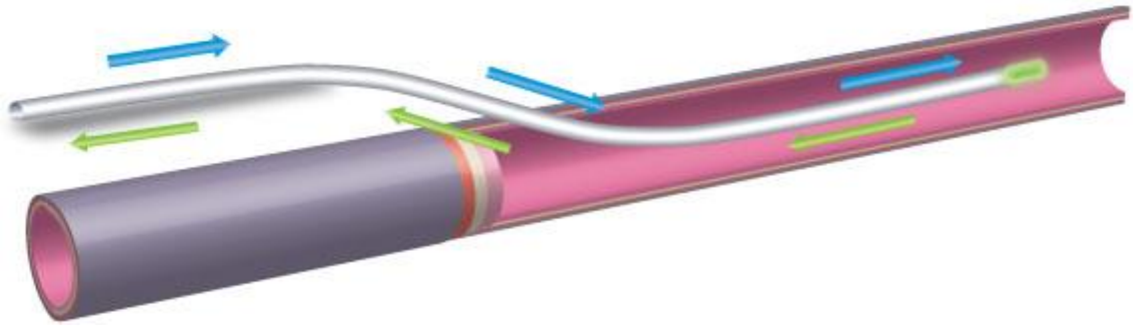

Figure 2.3: Glucath conceptual schematic [92].

2.10 VeraLight

VeraLight is a privately held company established in 2004. The company’s main product is the Scout DS which is a non-invasive diabetes screening system for the screening of Type-2 and prediabetes conditions. The device utilizes fluorescence spectroscopy for the measurement of advanced glycation end products (AGEs) in the skin of the forearm. Over the past decades, research has proven a correlation between the Skin AGEs and elevated glucose level and that is the basis of this device.

VeraLight has developed a proprietary algorithm that takes into account the variations in skin color, skin depth variations, and skin thickness to accurately measure the glucose concentration and deliver a meaningful result [86,93].

Figure 2.4: Scout DS glucose screening device [93].

CHAPTER III: SPECTROSCOPY

3.1 Introduction

The word spectroscopy refers to the investigative techniques based on the interaction of electromagnetic waves and matter. Spectroscopy covers the entire spectrum ranging from X-rays to radio frequency. Each region is characterized by its energy transfer. The energy transfers of each region are presented in the table below.

Table 3.1: Energy transfer corresponding to different spectrum region [99].

Region of Spectrum	Energy Transfer
X-rays	Bond Breaking
Ultraviolet/Visible	Electronic transition
Infrared	Molecular Vibration
Microwave	Molecular Rotation
Radiofrequencies	Nuclear Magnetic Resonance (Nuclear Spin)
	Electron Spin Resonance (Electron Spin)

The science of spectroscopy was originally started with Isaac Newton back in 1666 when he discovered that the white light coming from the sun can be broken down into continuous series of color lights. He called this phenomenon “Spectrum” this was the first time this term was used ever, after that more discoveries by many scientists contributed to this science [100].

For his experiment, Newton built an instrument that consisted of a small aperture to only pass one beam of light, a lens to collimate it, a prism to separate it, and a screen to display the spectrum.

After Newton and in the 1800, W Herschel demonstrated that the light radiating from the sun extended into the infrared region, and in 1801 J.W. Ritter demonstrated the existence of the ultraviolet light in the sun’s spectrum [100].

In 1814 Joseph Fraunhofer noticed fine dark lines crossing the sun’s spectrum when it is largely dispersed, these line are called Fraunhofer lines.

Even though Fraunhofer did not quite understand the origin of these lines, his discovery provided the quantitative foundation for spectroscopy.

The implementation of spectroscopy as a scientific tool didn’t begin until 1859 when Kirchhoff established that each element and compound has its own unique spectrum, and that by analyzing the spectrum of an unknown element, its chemical composition can be determined. This was the beginning of using spectroscopy as a scientific technique for studying atomic and molecular structure, and established the discipline of spectrochemical analysis for analyzing the composition of materials.

These techniques are the only tool used today to analyze terrestrial and astrophysical objects to determine their chemical elements [100].

After the discovery made by Kirchhoff, scientists collected a database of atomic spectral data, assigned characteristic lines to each element and accurately measured their wavelengths.

As the field of quantum mechanics developed, new light was shed on the science of spectroscopy and the structure of atom. In 1913 Bohr proposed that in an atom, the electron, bound by Coulomb force to the nucleus, which positively charged, moves in distinct circular orbits and that these discrete states do not radiate.

He proposed that light is only emitted when an electron at a higher state makes a transition to a lower state, and the energy lost by this transition is carried away by a photon whose energy is given by hv [100].

In the first half of the 20th century few discoveries were made that expanded the science of spectroscopy and led to the establishment of molecular spectroscopy.

Fist in 1918 R.W. Wood discovered the resonance radiation in vapors and then in 1928 C.V. Raman discovered the process of inelastic light scattering in molecules and the physical effect [100].

In 1924 Pauli proposed that the atomic nucleus have a small magnetic moment and in 1935 M. Schiiler and T. Schmidt proposed, after studying the hyperfine structure anomalies, the existence of a nuclear quadrupole moment [100].

Few spectrum analyzers were developed since 1868 to make spectroscopic measurements however the accuracy of the wavelengths measurement did not reach high accuracy until 1893 when Michelson built his analyzer.

Michelson analyzer employed an interferometer which consisted of reflective surfaces that cause the light to reflect and then interfere and upon interfering it produces a fringe pattern [100].

In 1905, Charles Fabry and Alfred Perot invented a new type of interferometer consisting of two parallel reflecting mirrors and by varying the distance between them different fringe patterns are produced, this interferometer carried their name and it is called Fabry-Perot interferometer.

Their results confirmed Michelson's conclusion that Row land's results weren’t accurate, and as a result in 1907 the 6438 Å line from a cadmium lamp as the primary standard of length was established to replace the standard meter. The new standard was more accurate, and it had the advantage of being able to be duplicated anywhere around the world. And in 1960 a new standard was established based on the orange line of ^{86}Kr at 6058 Å to replace the old one [100].

With the invention of LASER, a new era of spectroscopy started. The LASER with its high intensity light, narrow spectral width, and phase coherence opened a new interest in high resolution atomic and molecular spectroscopy [100].

Now a day the science of spectroscopy is divided to four subcategories [95]:

- Mass Spectroscopy
- Visible and Ultraviolet Spectroscopy
- NMR & ESR Spectroscopy
- Infrared Spectroscopy

3.2 Mass Spectroscopy

Mass Spectroscopy is an analytical technique used to determine the mass of atoms, molecules, nanoparticle, cell etc. by measuring the mass to charge ratio of charged particles. Mass spectroscopy cannot measure mass directly that is why an ionization step is required to create charged particles and then measure their mass to charge ratio.

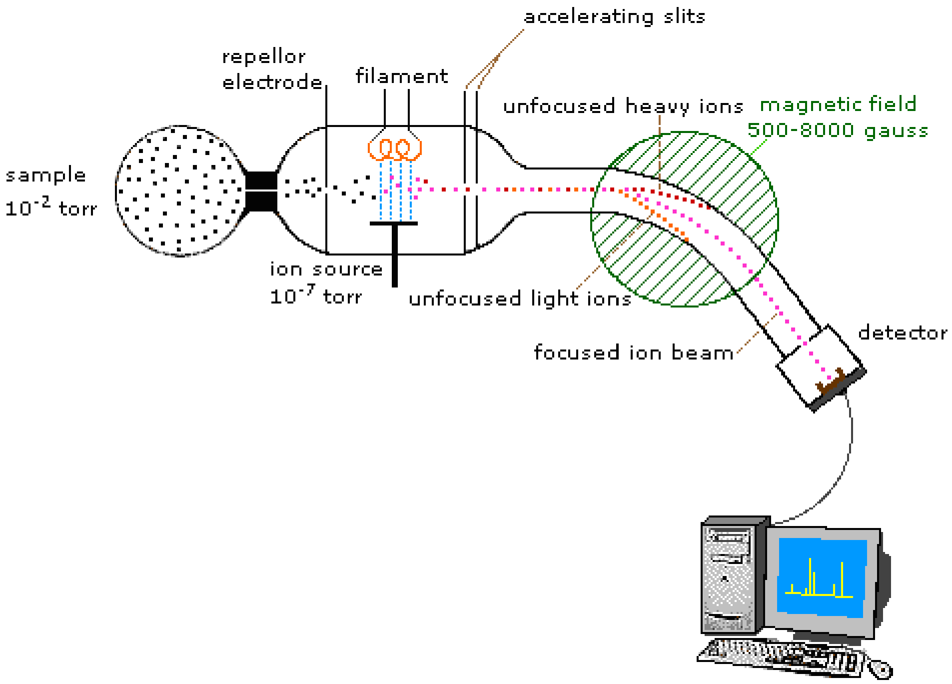

Figure 3.1: Mass Spectroscopy instrument diagram [101].

A Mass Spectroscopy instrument consists of three main components, an ion source, which converts gas phase molecules into ions, a mass analyzer or separator, which sorts the ions by their masses, and a detector, which measures the value and quantity of the charged particles and provides data for calculating the amount of each ion detected.

Many techniques have been developed over the years for Mass Spectroscopy measurements, below is a list and a brief description of each technique developed for each component [95].

3.2.1 Ionization technique

3.2.1.1 Electron Ionization.

Electron Ionization is the most common ionization technique used for mass spectroscopy. It works well for most molecules in the gas phase, but it does have its limitations. Because electron Ionization causes a great fragmentation it provides structural information of the molecule which helps to interpret its unknown spectra [95].

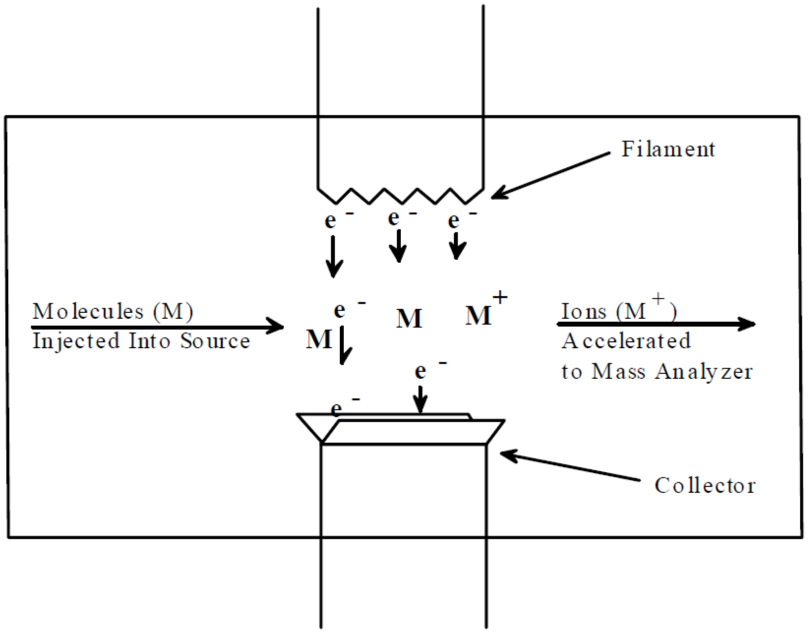

Figure 3.2: Electron Ionization [95].

As depicted in the figure above, the electrons used in the ionization are created by passing a high current in the filament to heat up after certain temperature the wire starts electrons and an electric field accelerates these electrons across the source and keeps a the beam of electrons flowing. As the molecule, in gas phase, passes through the high energy electrons beam, the molecule looses electron from its outer shell and becomes a positive ion [95].

If the electron energy is higher than the energy needed for ionization then, this results in molecule fragmentation where the number of fragments is determined by the ionization energy and the kinetics of the fragmentation pathways. Depending on the ionization energy different distribution of fragment ions can be observed [95].

This distribution is then interpreted to determine the mass spectra of the compound.

3.2.1.2 Chemical Ionization

Chemical Ionization is also called soft ionization because unlike the electron ionization this technique generates ions with minimal excess energy. Thus this technique produces more molecular ion and less fragmentation which makes it ideal for molecular mass determination [95].

In the chemical ionization a reagent gas is used and ionized in the source with an electron beam upon ionization the reagent gas creates a cloud of ions. These ions react with each other and produce adduct ions which are great proton donors.

When a molecule enters the source the adduct ions donate a proton to the molecule which becomes a positive ion [95].

3.2.1.3 Fast Atom Bombardment.

Fast Atom Bombardment employs high energy atoms to sputter and ionize the molecule in a one step. In this ionization technique, a beam of high energy rare gas is focused on sample, and upon impinging on the surface of the sample the high energy causes the molecules to sputter into the gas phase and ionize in one step. The exact mechanism of this process is not well understood, but since this technique doesn’t require any heating, it is well suited to study thermally sensitive compound that would otherwise decompose [95].

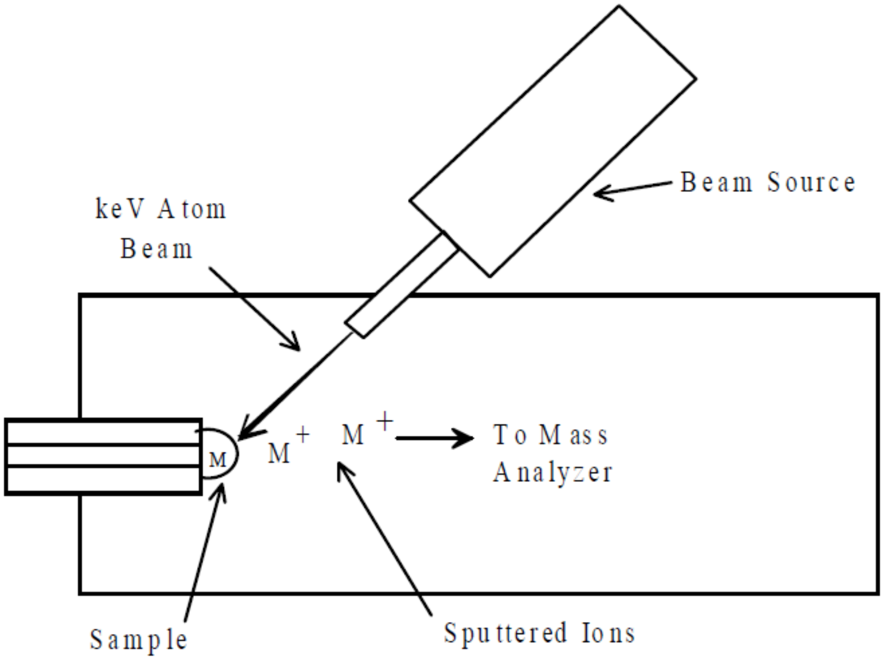

Figure 3.3: Fast Atom Bombardment Source [95].

3.2.1.4 Atmospheric Pressure Ionization and Electrospray Ionization.

Atmospheric Pressure Ionization technique uses the atmospheric pressure to ionize the sample and then transfer the ions into the mass spectrometer. Similarly to the fast atom bombardment these techniques are best used for thermally labile samples. For this technique the sample is prepared by dissolving it in an appropriate solvent and then the solution is launched into the mass spectrometer [95].

By using conventional inlets the solution increases the pressure in the source area of the mass spectrometer. Furthermore, the Joule-Thompson effect of the liquid when entering the vacuum causes the solution droplets to freeze. The sample then passes through a series of differentially pumped stages this method allows to keep a large pressure difference without using big vacuum pumps. In order to break up the formed clusters a drying gas is introduced in the process [95].

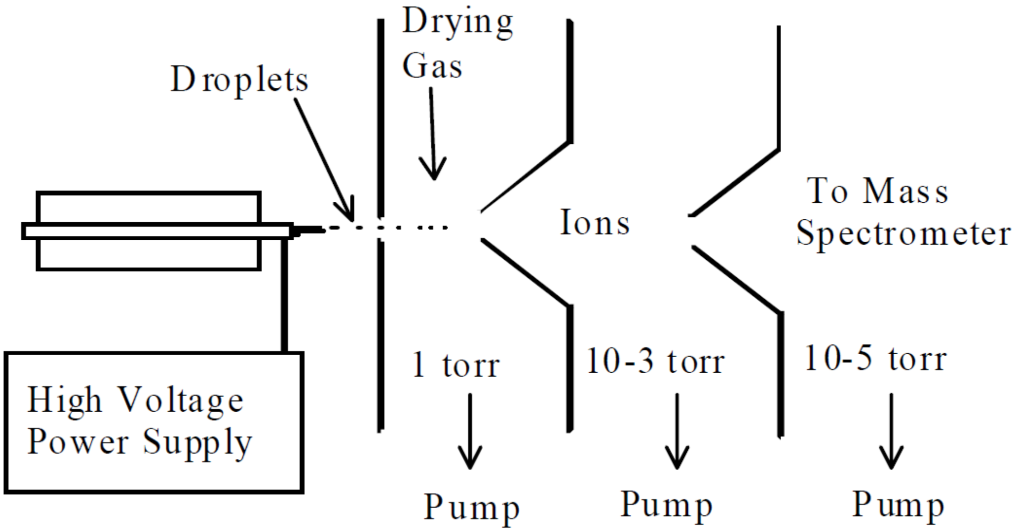

Figure 3.4: Electrospray Ionization Source [95].

The most common application of Atmospheric Pressure Ionization is electrospray ionization which implies using a large potential between the metal inlet needle and the first skimmer in the source [95].

3.2.2 Mass Analyzers

After the formation of ions in the source an electric field accelerates them to the mass analyzer where they are separated according to their mass to charge ratio. Mass Analyzers can be continuous or pulsed, only pulsed analyzers will be discussed here [95].

3.2.2.1 Time-of-Flight.

The time-of-flight mass analyzer is a sample analyzer that uses a fixed voltage and doesn't need a magnetic field. This analyzer only needs one fast ionization pulse to form ions which are then accelerated in the flight tube by an electric field formed between the backing plate and the acceleration grid [95].

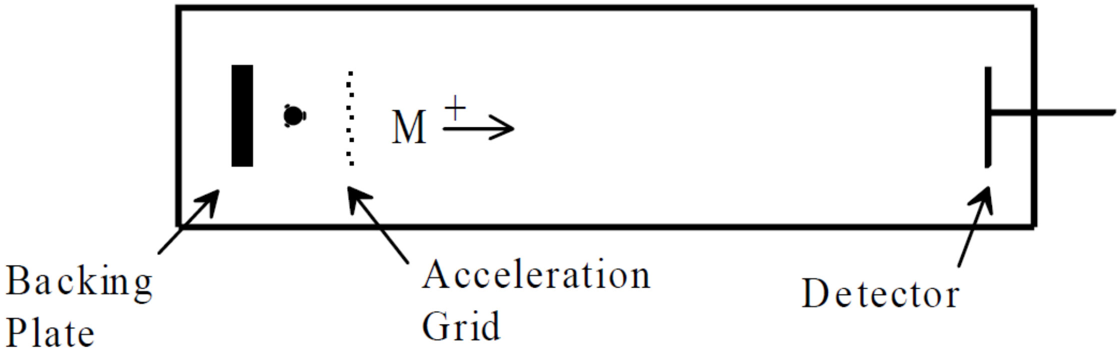

Figure 3.5: Time-of-Flight Mass Spectrometer [95].

3.2.2.2 Quadrupole Ion Trap.

The Quadrupole ion trap mass analyzer consists of a doughnut shaped ring electrode and two endcap electrodes as depicted in the figure below.

It is a newly developed mass analyzer with some special features such as high sensitivity and fast scanning. Since the quadrupole ion trap mass analyzer detects all the formed ions it exhibits high signal-to-noise ratio [95].

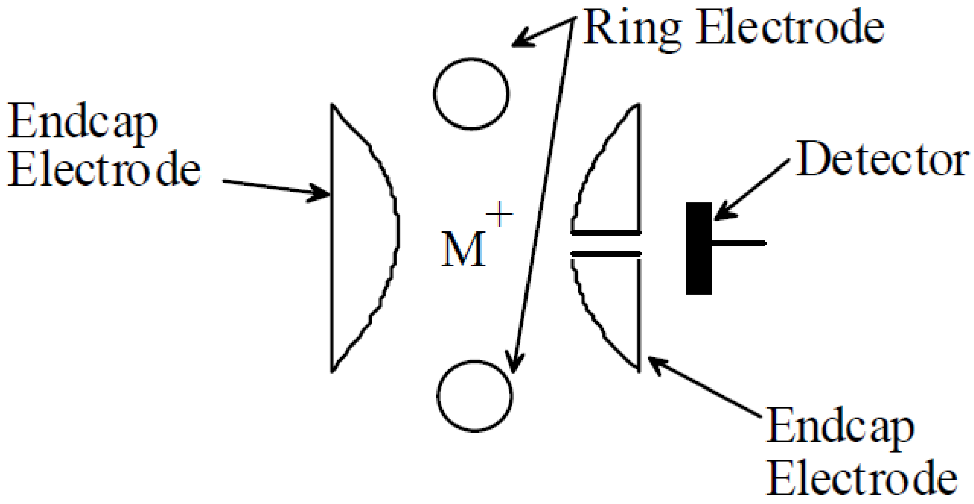

Figure 3.6: A cut-away of the Quadrupole Ion Trap Mass Spectrometer [95].

3.2.2.3 Ion Cyclotron Resonance

The Ion Cyclotron Resonance mass analyzer employs a superconducting magnet to trap ions in a small sample cell. The magnetic field created causes ions to travel in a circular path similar to the path of an ion in a magnetic sector, however the ions are traveling slower and the magnetic field is stronger. Due to this fact the ions are contained in the volume of the trap. After trapping them the ions are detected by measuring the signal at this cyclotron frequency [95].

This type of analyzer is very expensive and usually used for specialized research applications.

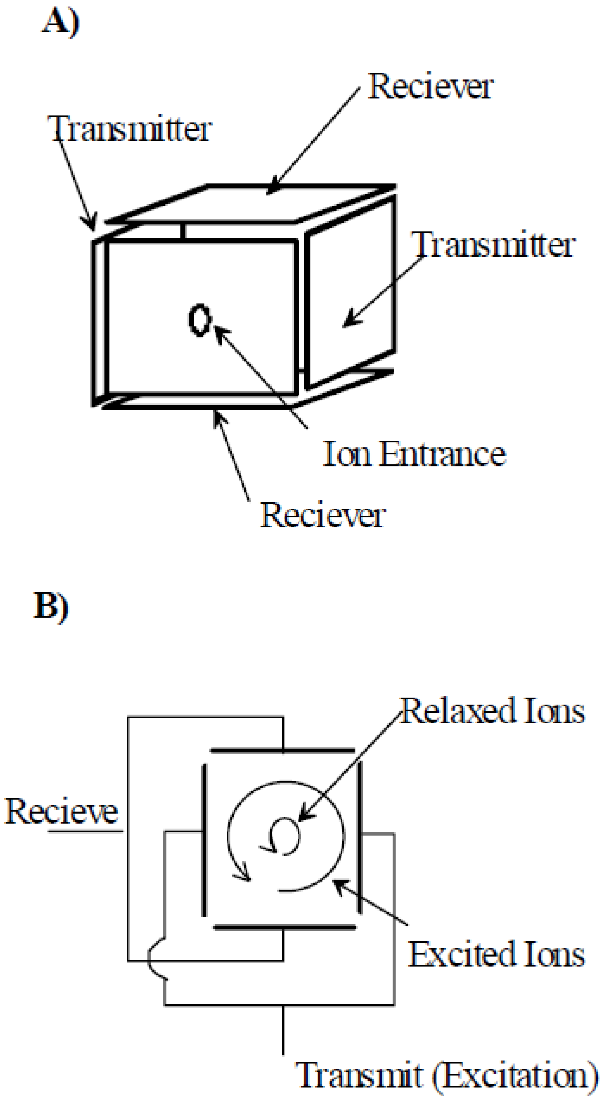

Figure 3.7: Ion Cyclotron Mass Spectrometer. A) main components, B) ion movement within the trap [95].

3.2.3 Detectors

The detector is selected based on the application requirement such as speed, dynamic range, gain, and geometry.

Faraday cup is used to collect ions and measure the current in large signal application. In some older instruments photographic plates were used to measure the number of ions at each mass to charge ratio.

Modern detectors amplify the ion signal using a collector like a photomultiplier tube. Other detectors are sufficiently sensitive to detect a single ion [95].

3.3 Visible and Ultraviolet Spectroscopy

The visible-ultraviolet spectroscopy covers the region of the spectrum ranging from 190 nm to 800 nm. Ultraviolet-visible spectroscopy observes the electronic transitions from one state to another allowing us to find out the wavelength and maximum absorbance of compounds.

By using Beer's Law: $A = \varepsilon bc$, where:

A = absorbance,
ε = molar extinction coefficient,
b = path length,
and c =concentration

We can determine either the concentration or the molar absorptivity depending on what variable is known. Since each compound has its own molar extinction, UV-Vis spectroscopy can be used to determine the identity of an unknown compound.

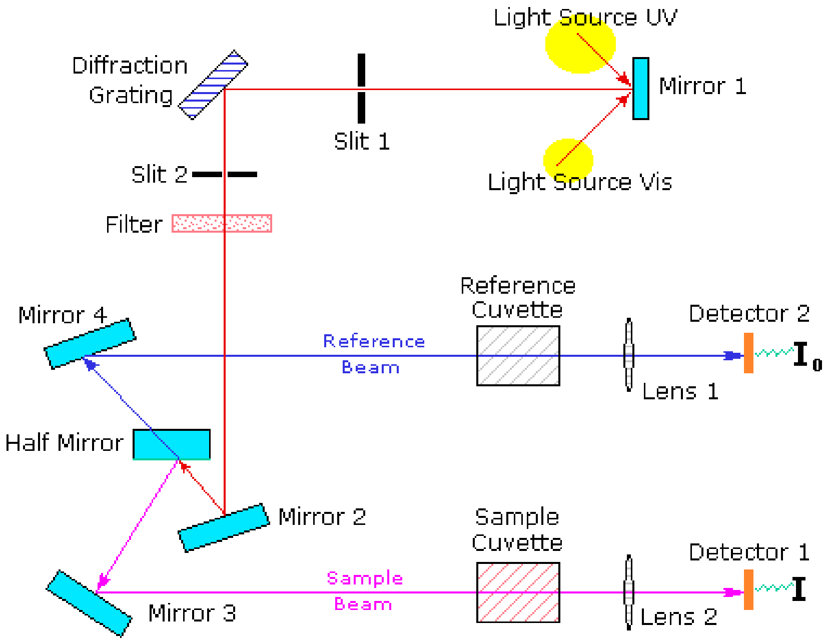

Figure 3.8: Typical UV-VIS spectrometer [97].

A typical diagram of a spectrometer is shown in the figure above. The spectrometer works as follows, a beam of light from a visible and/or UV light source is broken down into its different light wavelengths by a prism or diffraction grating. Each wavelength is then split into two beams of equal intensity by a half-mirrored device. One beam, the sample beam passes through a small transparent container containing the sample being analyzed.

The other beam, the reference beam, passes through an identical container containing only the solvent. The intensities of both beams are then measured by detectors and their ratio is plotted versus wavelengths. Since every compound has its own transmittance/absorbance profile, the compound is then determined by analyzing the graph [97].

3.4 NMR & ESR Spectroscopy

NMR stands for Nuclear Magnetic Resonance; NMR spectroscopy is used to determine the physical and chemical properties of molecules by making use of the magnetic properties of certain atomic nuclei [98].

NMR is based on the concept that many nuclei have spin and all nuclei are electrically charge. If nuclei are subjected to an external magnetic field, then an energy transfer is likely between a lower energy to a higher energy level [98].

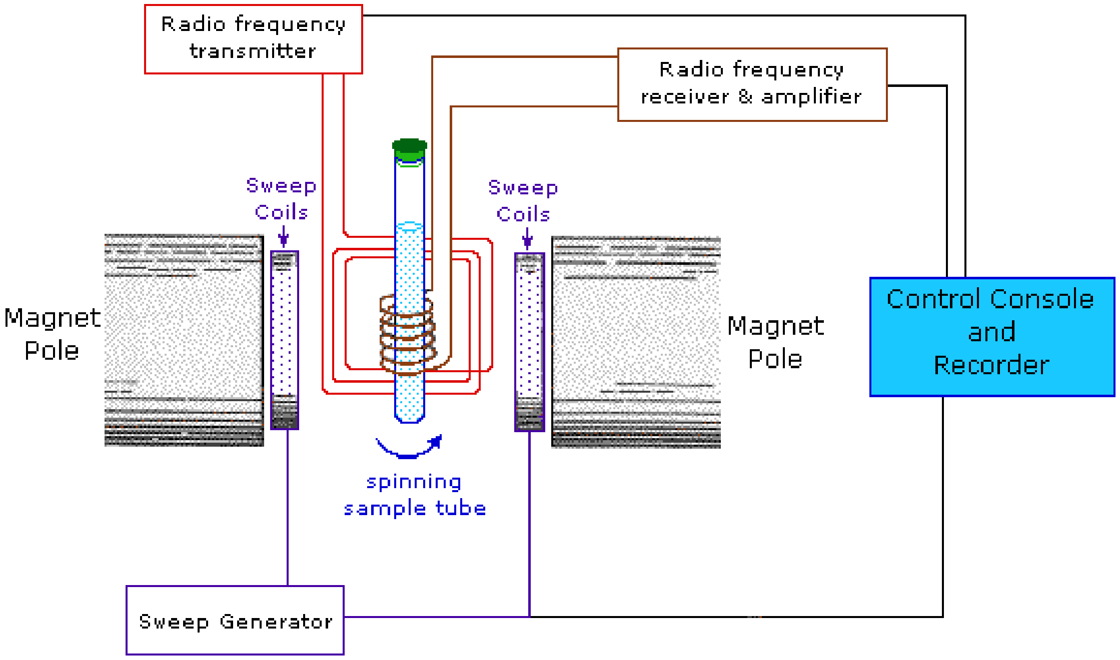

Figure 3.9: Diagram of NMR spectrometer [98]

This energy transfer occurs at a wavelength that corresponds to radio frequencies and when the spin returns to its lower level, energy is released at the same frequency. The signal that matches this transfer is then measured and processed in order to produce an NMR spectrum for the nucleus being studied [96].

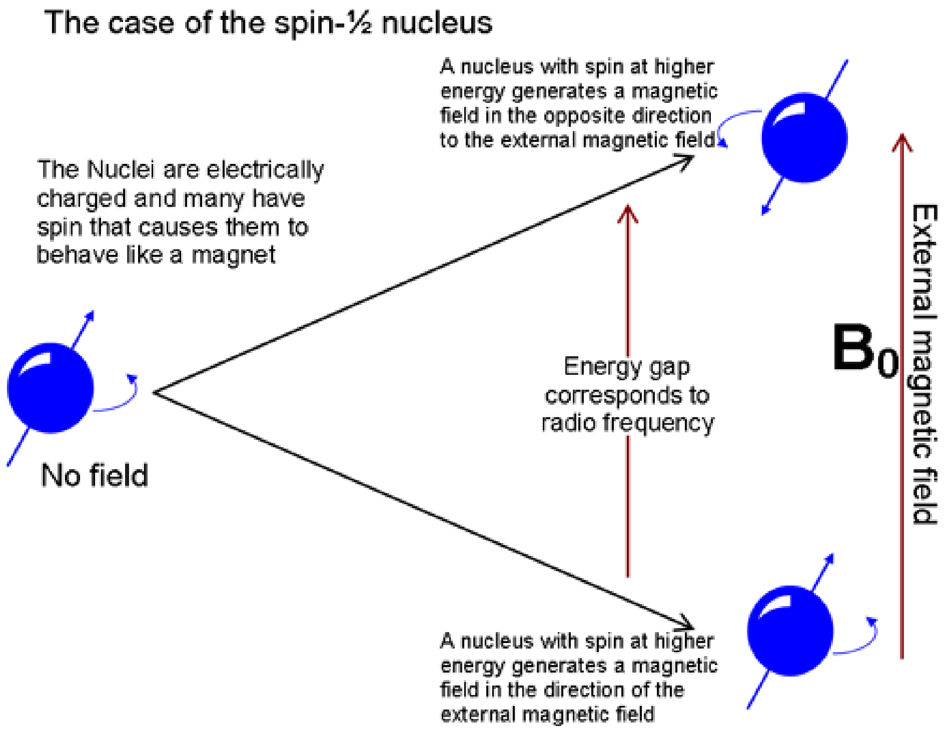

Figure 3.10: The basis of NMR [96]

ESR stands for Electron Spin Resonance, ESR spectroscopy is similar to NMR, and however in ESR the electron spins are excited instead of nuclear spins of NMR.

3.5 Infrared Spectroscopy

Infrared spectroscopy is a technique of molecular spectroscopy. This technique has been used in many fields and industries for a variety of measurements. For instance it is used to monitor certain gas species for environmental and industrial measurements, such as CO2, CH4 and CH2O. In the medical field it is used for the detection of toxic molecules and drugs. It is even used by law enforcement for the detection of explosives and hazardous material [19].

Infrared refers to the region of the electromagnetic spectrum ranging from 0.78 µm to 1000 µm. The infrared region is divided to three sub-regions near-infrared (NIR), mid-infrared (MIR), and far-infrared (FIR). Table 1 below shows the IR spectrum of each sub-region [20].

Table 3.2. Infrared regions spectrum range [20].

IR Sub-region	spectrum range (µm)
Near Infrared (NIR)	0.78 - 2.5
Mid Infrared (MIR)	2.5 - 50
Far Infrared (FIR)	50 – 1000

Molecular spectroscopy and consequently Infrared spectroscopy is based on the principle of molecular vibration. A molecule vibrates when bonds between its atoms stretch and bend.

Stretching is the change in inter-atomic distance along bond axis and it is divided to symmetrical and asymmetrical, where Bending is the change in the angle between two bonds. Bending is divided into four types, Rocking, Scissoring, Wagging, and Twisting [21].

For a molecule to absorb an infra-red radiation, it must be active in the IR region. That is when exposed to IR radiation; a change in the net dipole moment must occur [21]. A molecule will have an electric dipole moment when two adjacent atoms in the molecule have different charge, a positive charge (+ e) and a negative charge (- e). The electric moment is defined as $\mu = e \times d$ where e is the magnitude of charge at either end of the dipole, and d is the distance between the centers of + e and – e charge [23].

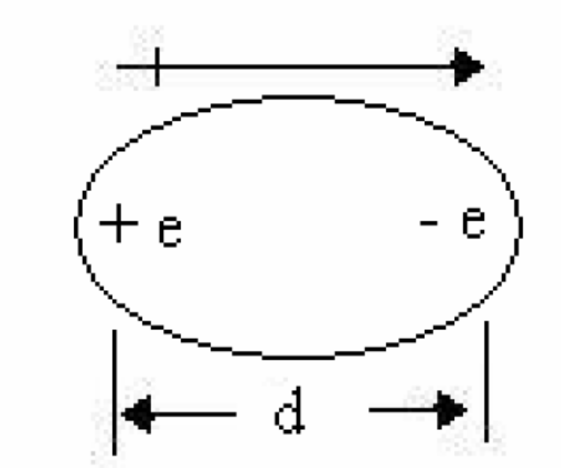

Figure 3.11: dipole moment direction [23].

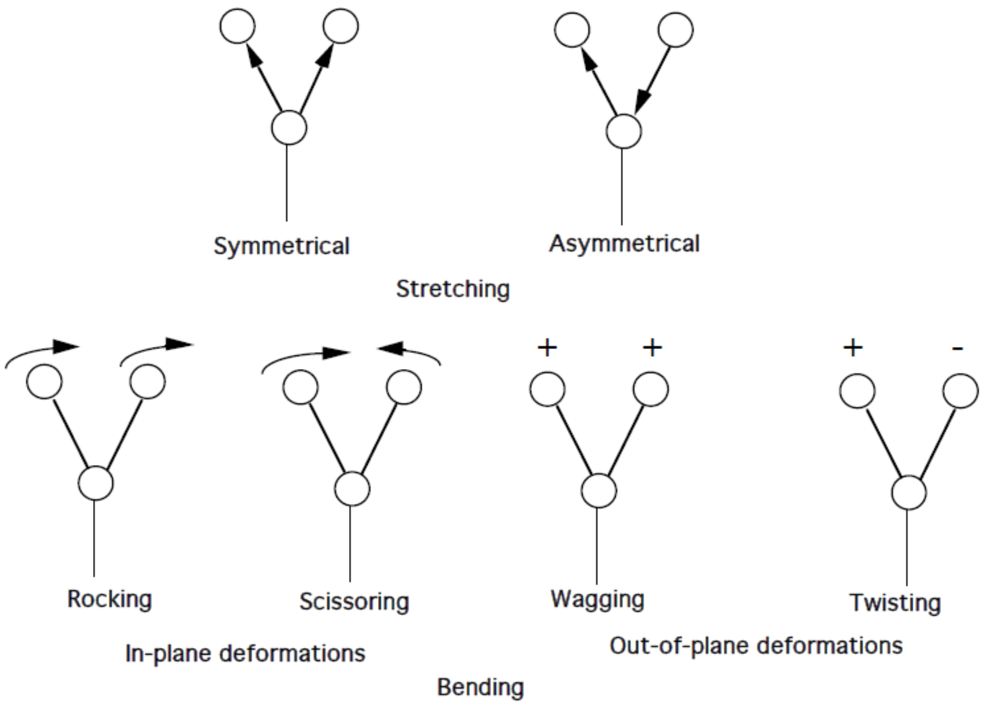

Figure 3.12: Different vibration modes of a molecule [23].

3.5.1 Water Molecule Vibration and IR Spectra

For example the water molecule has 3 modes of vibration illustrated in figure 3, those vibration modes result in the infrared spectra shown in figure 4 [24].

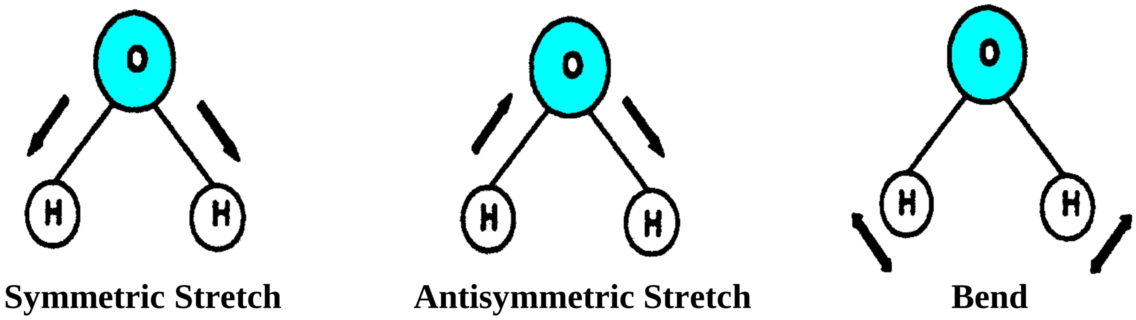

Figure 3.13: H2O molecule vibration modes [24].

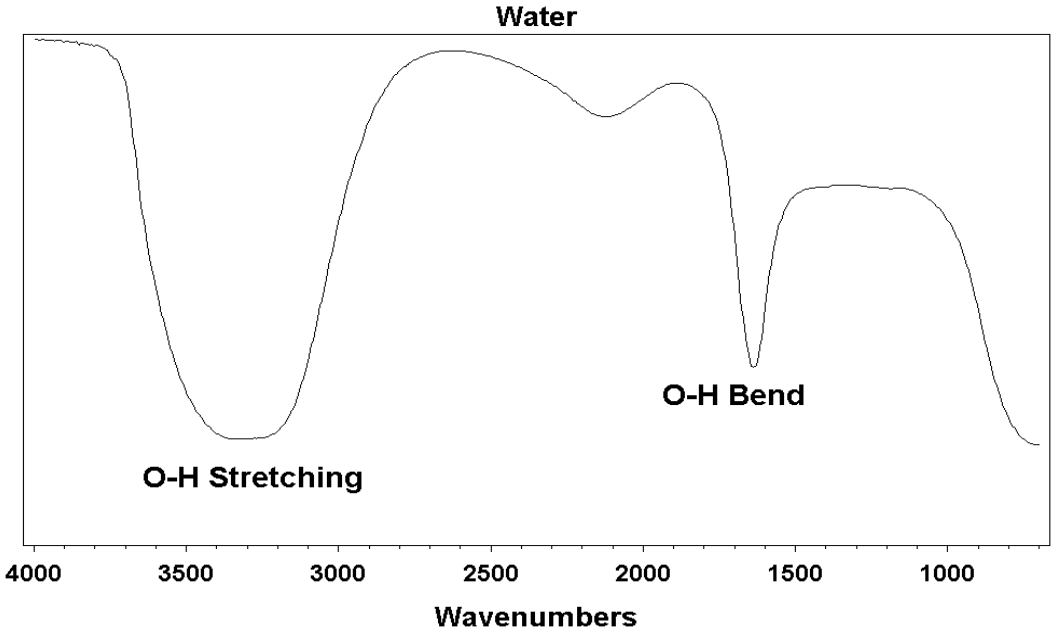

Figure 3.14: H2O molecule absorption spectra and its correlation with the vibration modes [24].

CHAPTER IV: INFRA-RED SOURCES

4.1 Introduction

Infra Red (IR) sources are made from different materials, metal and ceramic, which is upon heating start glowing and emitting light of broad spectrum [25].

The energy radiated by the IR source per unit area is called the body's “emittance” R and it is proportional to IR source temperature [26-28]. The spectral emittance of these sources follows Planck’s law [25].

$$R_{\lambda} = \frac{8\pi hc}{\lambda^{5}(e^{hc/\lambda kT} - 1)}$$ Where:

R = the radiant power emitted per unit radiating surface area per unit wavelength ($W\,m^{-2}$)
c = Speed of light
h = Planck’s constant
λ = Wavelength
k = Boltzman constant
T = Temperature (K)

The following graph shows the spectral emittance of an ideal IR source as temperature increases.

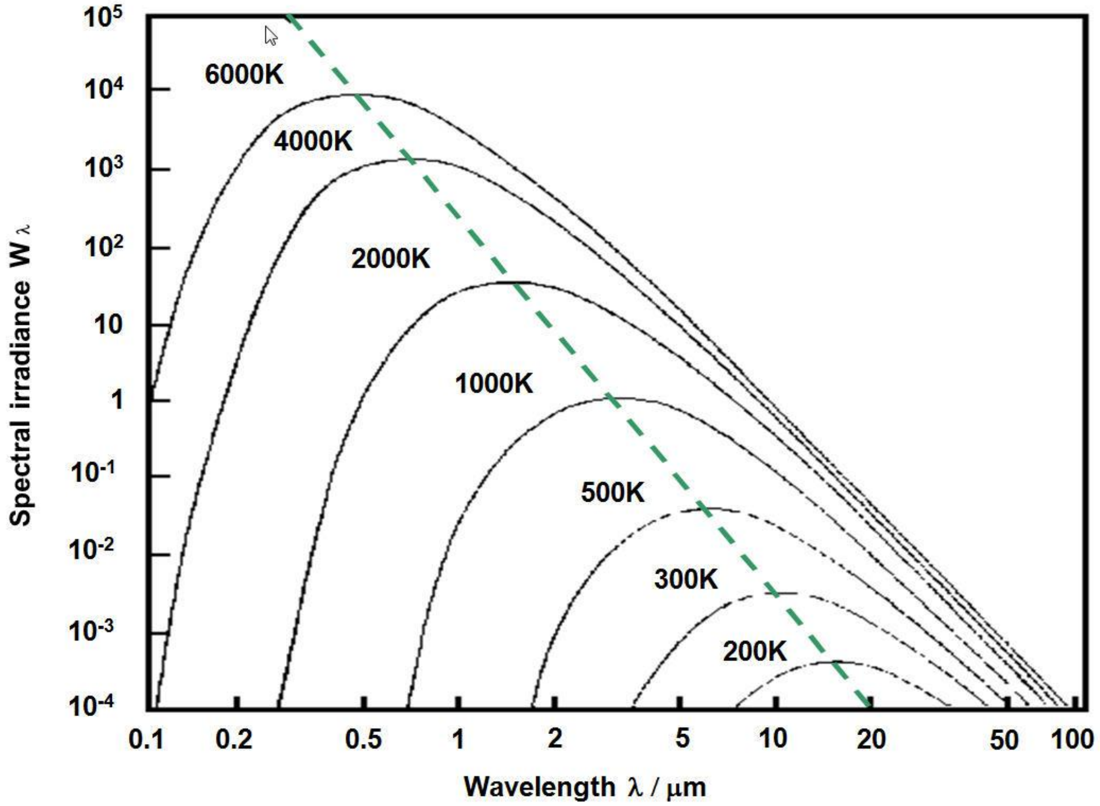

Figure 4.1: The spectral emittance of an ideal IR source with different temperatures.There are many types of IR sources used in spectroscopy; each has its uniqueness in terms of size, emissivity, and temperature [33].

The IR sources are discussed below.

4.2 Globar

The Globar is most used IR source in FTIR. It is made of silicon carbide rod and it is electrically heated by passing a current through it [29, 30]. The Globar can reach a temperature as high as 1300 K. However, the high out power can result in excessive heat being dissipated in the machine which requires water cooling to protect the electrodes from damage [29, 30].

4.3 Nernst Glower

The Nernst Glower is one of the original IR sources used in spectroscopy. It is composed of rare earth metal oxides, such as zirconium and yttrium [29, 30].
The spectral emittace is close to a black body with a nominal operating temperature of 1800 K. One drawback of this source is that it has a negative coefficient of electrical resistance, meaning its resistance decreases as the temperature increases to overcome this problem a ballast resistor must be used to regulate the output [29,30].

4.4 Ceramic Source

The ceramic source known also *Opperman* source consists of a ceramic tube with a rare metal oxide wire located in its center. The wire is electrically heated which in turn heats the ceramic tube emitting radiation [29].

4.5 Metal Filaments source

Simply this is an incandescent light bulb without its glass cover, because the glass cover limits the emission spectrum to 4 μm [29-31]. These filaments are electrically heated and they can reach temperature as high as 2800 K.
One disadvantage of using this source is the short lifetime due to thermal stress and oxidation [29-31].

4.6 Planar sources

These sources are made of a thin film structure fabricated on a Si wafer with an integrated heating element. These sources are electrically heated and they can reach temperature as high as 1025 K [31,32].

CHAPTER V: DETECTORS

5.1 Introduction

The detectors used to detect IR energy are divided to two main categories of photo-detectors and thermal detectors.

5.2 Photo-detectors

Photodetector is an optical device that converts the detected light into electrical signal such as voltage or current. Photodetectors are made of semiconductor materials of a specific band gap and structured in a specific way [37-39].

Semiconductors are different from insulators and metals by the fact that their conduction band is relatively close to the valence band which makes their electron excitation possible under certain conditions.

For instance when the energy ($h\upsilon$) of the incident photon is greater than the band gap energy, then the photon has enough energy to excite an electron from the valence band to the conduction band leaving behind a positive hole.

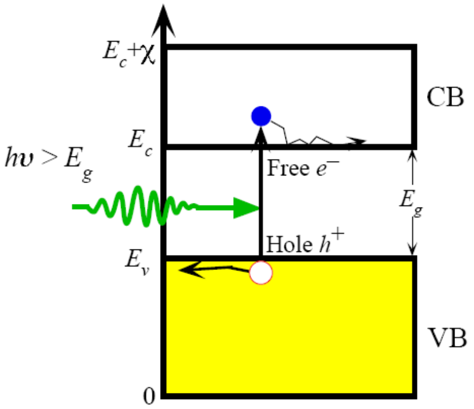

Figure 5.1: Illustration of an atom band gap [34].

The band gap energy is proportional the photon wavelength as depicted by equation 1 [34].

$$E_g = \frac{hc}{\lambda} \qquad (1)$$ where:

h = Planck’s constant
c = speed of light
λ = photon wavelength

For infrared detection Quantum Well Infrared Photodetectors (QWIP*)* are the commonly used photodetectors in spectroscopy.

5.2.1 Quantum Well Infrared Photodetectors (QWIP)

The concept of detecting light by using quantum wells has been studied comprehensively for over 2 decades. Quantum wells are made by sandwiching a very thin layer, tens of nanometers, of semiconductor material between two semiconductors of wider band-gap. Since the thin layer material has a smaller band gap its electrons are thought of as confined in a “well” and the other two layers are the “barriers” [37-40].

The operation of the original quantum well was based on the absorption of the IR radiation by the free carriers that are trapped in the well layer. However the detection of the new infrared quantum well detectors is based on the intersubband transition in the well [38-40].

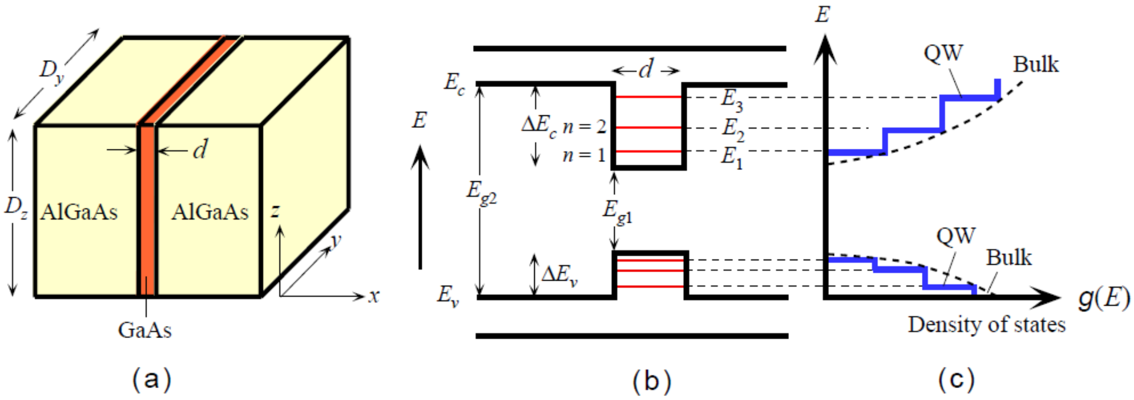

Figure 5.2: (a) Schematic illustration of a quantum well (QW) structure where a thin layer of GaAs is sandwiched between two semiconductors (AlGaAs) of wider bandgap. (b) The conduction electrons in the GaAs layer are confined by ΔEc and their energy is quantized by a small length *d* in the *x*-direction. (c) The density of states of a two-dimensional QW. The density of states is constant at each quantized energy level [34].

If we assume the growth direction is along the x axis, as in the figure above, then we can say that the conduction electrons are confined in the x direction and they are free to move in the other two dimensions. Since the well layer is very thin, the movement of electrons is quantized in the growth direction and the energy levels become discrete and called subbands [37-37].

The energy level at quantum level n is given by:

$$E_n = \frac{h^2 n^2}{8 m_e^* d^2}$$

And the intersubband transition energy between the lowest and first excited state is given by $E_2 - E_1 = \frac{3h^2 n^2}{8m_e^* d^2}$

Where h = Planck's constant
n = the quantum level
D = the well width
m_e^* = the electron effective mass

The main disadvantage of QWIPs is their high dark current which necessitates cooling the detector to temperature around 65 K or even below to eliminate any background interference [41].

5.3 Thermal Detectors

Thermal detectors are devices that convert the detected light into change in temperature. They are made of materials whose physical properties change due to change in temperature. There are two common thermal detectors:

Bolometers, whose resistance changes with temperature.

Pyroelectric detectors, whose surface charge changes with temperature.

5.3.1 Bolometer

Bolometer is a thermal detector used to measure the energy of incident radiation; it is capable of measuring a wide range of spectrum even though it is mostly used in longwave detection applications i.e astronomy [46].

As illustrated in the figure below, a bolometer consists of a heat absorbing material with a heat capacity C at a given temperature T. It is then thermally connected with conductance G to a heat sink with temperature T_0. The bolometer contains a resistive thermometer made of semiconductor material such as germanium [47].

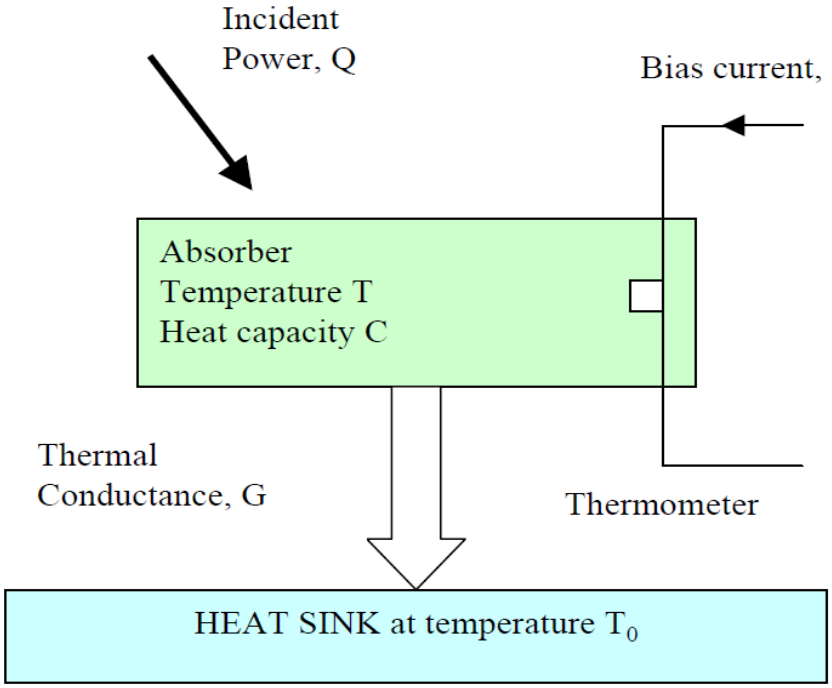

Figure 5.3: Structure of a bolometer [9].

The incident radiation causes the temperature in the absorbing material to rise proportionally to its energy according to the following equation [43,44]:

$$\Delta T = T - T_0 = E/C$$

As the temperature decreases because of the heat sink, it decays as follows [43,44]:

$$\tau = {}^{C}/_{G}$$

And as the temperature changes, the bolometer resistive material changes according to the following equation [43,44]:

$$R = R_S e^{(T_g|T)^{1/2}}$$

Where R_S is the resistance parameter (Ohms),R is the resistance (Ohms), T is the temperature of the resistor, and T_g (K) is the material band gap temperature.

The value of $\left(T_g \middle| T\right)$ is called the material parameter and is given the symbol δ. The temperature coefficient of resistance is defined by [43,44],

$$\alpha = \frac{1}{R}\frac{dR}{dT}$$

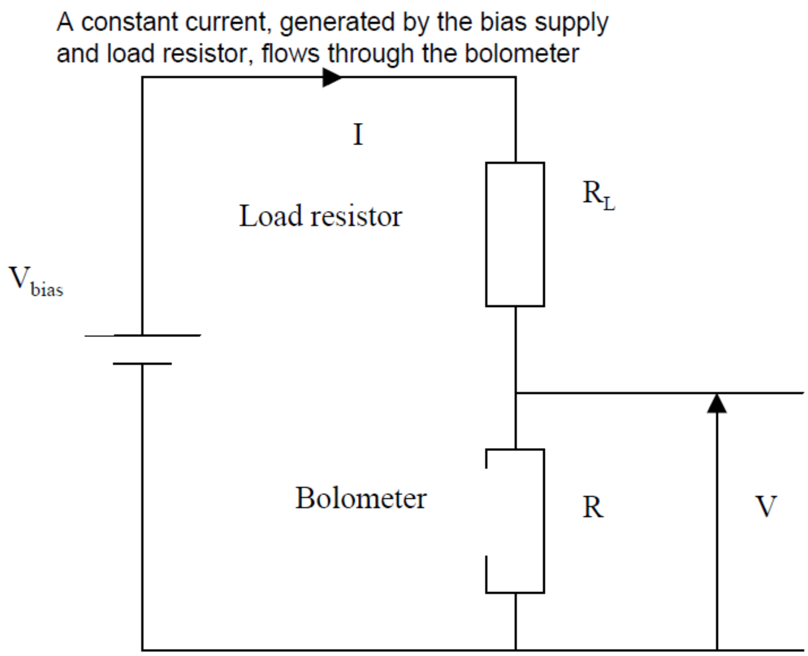

Figure 5.4: Bolometer circuit readout [42].

The typical bolometer readout circuit is illustrated in Figure. The bolometer is usually biased with a constant DC current I and as the current passes through the Bolometer resistance, it generates voltage across the resistance. The voltage can then be read with and ADC and correlated to the incoming energy.

5.3.2 Pyroelectric

Pyroelectric detector is another form of photo-detectors they are made of pyroelectric crystals, such as Lithium Tantalate ($LiTaO_3$) and Barium Titanate ($BaTiO_3$), capable of converting the change in temperature into electric signal [48-49].

The pyroelectric effect was first discovered in the 18th century in tourmaline crystals and in the 19th century Rochelle salt was used to fabricate pyroelectric sensors [36,50].

A pyroelectric material is composed of a large number of randomly oriented tiny crystals called crystallites. Those crystallites behave much like an electric dipole. When those crystallites go through a temperature change, they become polarized and an electric charge exists on the surface of the crystal.

However in order for any pyroelectric material to exhibit a pyroelectric effect, it must be operated below a certain temperature know as Curie point, above which the crystallites lose their dipole moment [36,50].

The magnitude of electric charge resulting from change in temperature is given by equation (3) [36,49]:

$$\Delta Q_a = A\mu(T_a, \Delta W) \qquad (3)$$ where:

μ = Dipole moment per unit volume
A = area
Ta = Temperature
ΔW = Thermal energy absorbed by the material

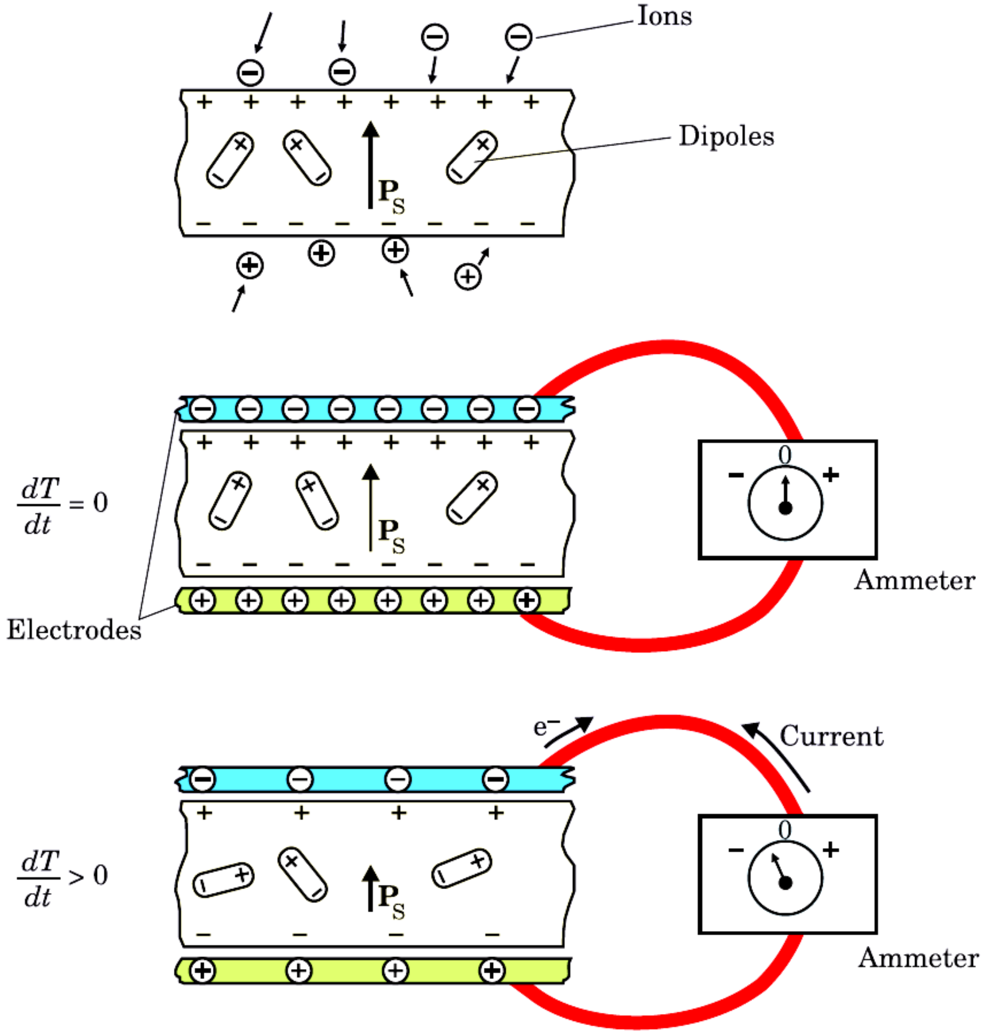

Figure 5.5: (Top) a pyroelectric crystal with an intrinsic dipole moment, (Middle) A pyroelectric crystal with electrode attached on each side, with no change in temperature there is no current flow. (Bottom) a change in temperature causes instantaneous polarization and flow of current [51].

In order to collect the charge, pyroelectric sensors are fabricated in thin films with electrodes on each side. The charge and voltage coefficients of a pyroelectric sensor can be described in equations (4) and (5) respectively [36]:

$$P_Q = \frac{dP_s}{dT} \qquad (4)$$

$$P_V = \frac{dE}{dT} \qquad (5)$$

Where:

Ps = Spontaneous polarization (electric charge)
E = Electric field strength
T = Temperature in K

Both coefficients are related the electric permittivity, ε_r, and dielectric constant, ε_0 as follows [3]:

$$\frac{P_Q}{P_V} = \frac{dP_s}{dE} = \varepsilon_r \varepsilon_0 \qquad (6)$$

Since the pyroelectric material is dependent on the change in temperature then charge and voltage changes can be described by equations (7) and (8) respectively:

$$\Delta Q = P_Q A \Delta T \qquad (7)$$

$\Delta V = P_V h \Delta T$ (8) where h is the thickness of the material

Now capacitance is defined as:

$$C_e = \frac{\Delta Q}{\Delta V} = \varepsilon_r \varepsilon_0 \frac{A}{h} \qquad (9)$$

Now the above equations can be rearranged as follows:

$$\Delta V = P_Q \frac{A}{C_e} \Delta T = P_Q \frac{\varepsilon_r \varepsilon_0}{h} \Delta T \qquad (10)$$

It is obvious from equation (10) that the output voltage is proportional to the change in temperature and the charge coefficient and inversely proportional to the film thickness.

CHAPTER VI: FABRY-PEROT INTERFEROMETER

6.1 Introduction

The Fabry-Perot interferometer is named after two French physicists, Charles Fabry and Alfred Perot, who in the late 1800 published a paper describing a device that became to be known Fabry-Perot interferometer [52,18].

The Fabry-Perot interferometer is an optical resonator formed by two parallel reflective surfaces separated by a fixed distance in a specific medium, such as air.

6.2 Fabry-Perot Applications

The Fabry-Perot interferometer has been used in many applications ranging from imaging spectroscopy [53] to optical filters [54], the most common are listed below.

6.2.1 Dichroic Filter

Dichroic filters are the most common application of Fabry-Perot, in which multi-layers of dielectric layers are deposited on a glass surface to allow only certain wavelengths of light to pass through and reflect the unwanted spectrum. Unlike absorptive filters, these filters transmit rather than absorb the unwanted spectrum, thus they transmit more light, stay cool, and don’t burn out.

6.2.2 Telecommunication Networks

Telecommunication networks that use wavelength division multiplexing have an add-drop multiplexer which made of Fabry-Perot etalon. This multiplexer can combine several wavelengths of data into a single light beam; and simultaneously, it can drop or remove other light signals from the stream of data and direct them to other network routes [102].

6.2.3 Optical wavemeter

An optical wavemeter is a made of a number of Fabry–Pérot interferometers with with different free spectral ranges. The beam is passed through a lens to diverge it and the distance between two bright lines is then recorded by an array of detectors [105].

6.2.4 Single Mode LASER

Etalons are used to build single-mode lasers. A LASER generally produces light over a range of wavelengths instead of a single wavelength; this broad range of light corresponds to multi-cavity modes.

By employing an etalon into the laser cavity, that has a specific free-spectral range, all unwanted frequencies or wavelengths can then be suppressed, thus changing the operation of the laser from multi-mode to single-mode.

6.2.5 Zeeman-effect detection

A Fabry–Perot etalon can be used to detect the Zeeman-effect. The Zeeman Effect is observed when there is a magnetic field to influence the atomic energy levels under such influence the atomic energy levels as well as the spectral lines split to larger number. By using Fabry–Perot etalon the spectrometer becomes sensitive enough to detect the spectral lines that are too close together to distinguish with a normal spectrometer [104].

6.2.6 Astronomy

In astronomy the etalon is used to measure the intensity of light, emitted by objects in the space, as a function of wavelength. The data allow astronomers to understand the physical properties and the motion of these objects in the space.

6.2.7 Gravitational wave detection

Gravitational waves are ripples of space-time and they are the basis of the theory of relativity. By using Fabry–Perot cavity one can store photons for a very short period of time as they bounce back and forth between the mirrors.

This increases the time of interaction between a gravitational wave and light, resulting in a better sensitivity at low frequencies. This principle is used by detectors such as LIGO, which consist of a Michelson interferometer with a Fabry–Perot cavity with a length of several kilometers in both arms [103].

6.3 Operation and Mirrors Material

A typical Fabry-Perot interferometer and its transmission are illustrated in Figure 6.1(a) and 6.1(b) respectively. Assuming M1 and M2 are two mirrors perfectly parallel to each other, and then the light waves in the cavity reflect back and forth between M1 and

M2. Those light waves interfere constructively and destructively resulting in standing EM waves [55].

If we assume that E_oP_1 is the wave representing the direction of the incident wave, then this wave upon impinging on the mirror M_1 divides into two waves, a reflected wave in the direction of $P_1E_1^{'}$, and a transmitted wave in the direction of $P_1P_1^{'}$.
The transmitted wave impinges on mirror M_2 at angle θ, and it is as well divided into two waves, one transmitted in the direction of $P_1^{'}E_1^{'}$, and one reflected in the filter in the direction of $P_1^{'}P_2$.

This process of reflection/transmission of the wave continues indefinitely as depicted in figure 1-(a) below. The total transmitted light will be the sum of all transmitted waves.
However since the transmitted waves are not in phase, we need to determine their phase difference.

In optics the phase shift corresponds to the difference in optical paths which is for E_1 and E_2 is given by [55, 70, 71]:

$$n\overline{P_1^{'}P_2P_2^{'}} - \overline{P_1^{'}Q_1} = \frac{2nd}{\cos\theta} - \frac{2d}{\cos\theta} = \frac{2nd}{\cos\theta} - \frac{2d}{\cos\theta}\sin\theta\sin\phi = \frac{2nd}{\cos\theta} - \frac{2d}{\cos\theta}\sin\theta(n\sin\theta)$$

$$= \frac{2nd}{\cos\theta}(1-\sin^2\theta) = 2nd\cos\theta$$

The phase difference is given by:

$$\delta = \left(\frac{2\pi}{\lambda}\right)2nd\cos\theta$$

The incident electromagnetic wave can be described as [56]:

$E(t) = E_0 e^{-iwt+ikz}$, where $w = \frac{2\pi C}{\lambda}$, $k = \frac{2\pi}{\lambda}$.

If both mirrors have the same reflectivity R, then the total transmitted field can be written as:

$$E_T = \frac{E_0(1-R)e^{-i(wt-\delta_0)}}{1-R*e^{i2\delta}}$$

and the transmitted intensity will then be [70,71] :

$$I_T = E_T^2 = \frac{I_0(1-R)^2}{1+R^2-2R\cos 2\delta} = \frac{I_0(1-R)^2}{1+R^2-2R+2R(1-\cos 2\delta)}$$

$$= \frac{I_0(1-R)^2}{(1-R)^2+4R\sin^2\delta}$$

This can be re-written as:

$$I_T = \frac{I_0}{1+F\sin^2\delta} \qquad where$$

$$F = \frac{4R}{(1-R)^2}$$

Therefore, we can conclude that the transmitted intensity is a periodic function of the phase shift and when the mirror reflectivity is very high, then transmission occur only when the following condition is satisfied [55] :

$$\delta = \frac{2\pi nd\cos\theta}{\lambda} = m\pi$$

Assume θ = 0, and n=1, then $\delta = \frac{2\pi nd}{\lambda} = m\pi \Rightarrow m = \frac{2d}{\lambda}$, where m is an integer that corresponds to the cavity mode.

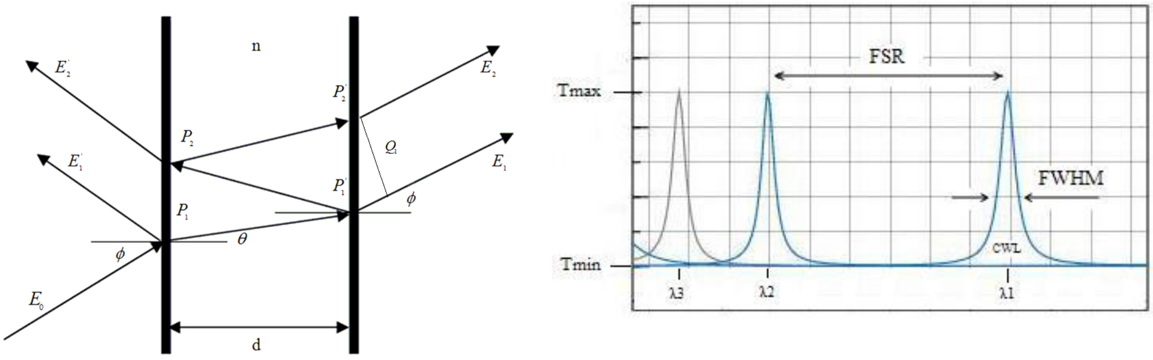

(a) (b)

Figure 6.1: (a) Schematic of an FPI. *M1* and *M2* are the two mirrors; d is the distance between the mirrors; ϕ is the angle of incident light, and θ is the phase shift at reflection. (b) Transmission spectrum of an FPI.

The transmittance spectrum of a FPI is illustrated in figure-1 (b) and described by the airy-function in equation (1).

Assuming the two reflectors have the same reflectance R and the same absorbance A, the transmission T can be described as follows [6]:

$$T = \left(1 - \frac{A}{(1-R)}\right)^2 \frac{1}{1 + \left(\frac{4R}{(1-R)^2}\right)\sin^2\left(2\pi n d \frac{1}{\lambda}\cos\theta - \phi\right)} \qquad (1)$$

To simplify the discussion, we assume that the angle of incidence is zero and the phase change on reflections is π, then equation (1) becomes:

$$T = \left(1 - \frac{A}{(1-R)}\right)^2 \frac{1}{1 + \left(\frac{4R}{(1-R)^2}\right)\sin^2\left(\frac{2\pi n d}{\lambda}\right)}$$

The transmission peaks occur when the following condition is satisfied:

$$\frac{2\pi n d}{\lambda} = m\pi \Rightarrow \lambda_m = \frac{2nd}{m} \qquad (2)$$

The spectral resolution of a FPI, which determines the spectral bandwidth (FWHM), is described in equation (3) [6].

$$FWHM = \frac{1}{2d\pi}\frac{1-R}{\pi\sqrt{R}} \qquad (3)$$

The spectral distance between two adjacent peaks or resonant wavelengths is called the Free Spectral Range (FSR), and the ratio of FSR and FWHM is called the Finesse and it is described in equation (4) [57]:

$$\tilde{F} = \frac{FSR}{FWHM} = \frac{\pi\sqrt{R}}{1-R} \qquad (4)$$

The performance of a Fabry-Perot interferometer depends on the reflectivity of the mirrors. The higher the reflectance the sharper and narrower the transmission peaks of the filter. Therefore, as R increases FWHM decreases.

There are two commonly used materials in the fabrication of optical mirrors, metal thin film, and multilayer dielectric coatings.

6.3.1 Metal Thin Film Mirrors

Metallic mirrors consist of a thin layer of a metal coated on a substrate. Metallic mirrors are easy to fabricate and they have a good reflectance over a long range. However they require periodic maintenance and suffer from absorption loss, figure 2 below shows the reflectance of the most common metals used as reflective mirrors [58].

Aluminum is the most commonly used material simply because it has a very good reflectivity in the ultraviolet, visible and infrared spectrum and because of its strong adherence on most material including plastics. However the performance of an aluminum mirror falls gradually over time and that is due to oxidation and collection of dirt and dust on the surface that sometimes cannot be easily cleaned without damaging the film, in this case a recurring recoating is required [58].

Silver is similar to Aluminum in terms of easiness to manufacture; however it is damaged rather quickly upon exposure to the atmosphere due to the formation of silver sulphide. And similar to Aluminum a periodic recoating is needed to mitigate the problem [58]. Gold is probably the best material to use as mirror in terms of maintenance because it doesn’t require recoating. However gold film suffers from being soft, easily scratched, and difficult to adhere on the substrate without an underlayer of Chrome or Nichrome.

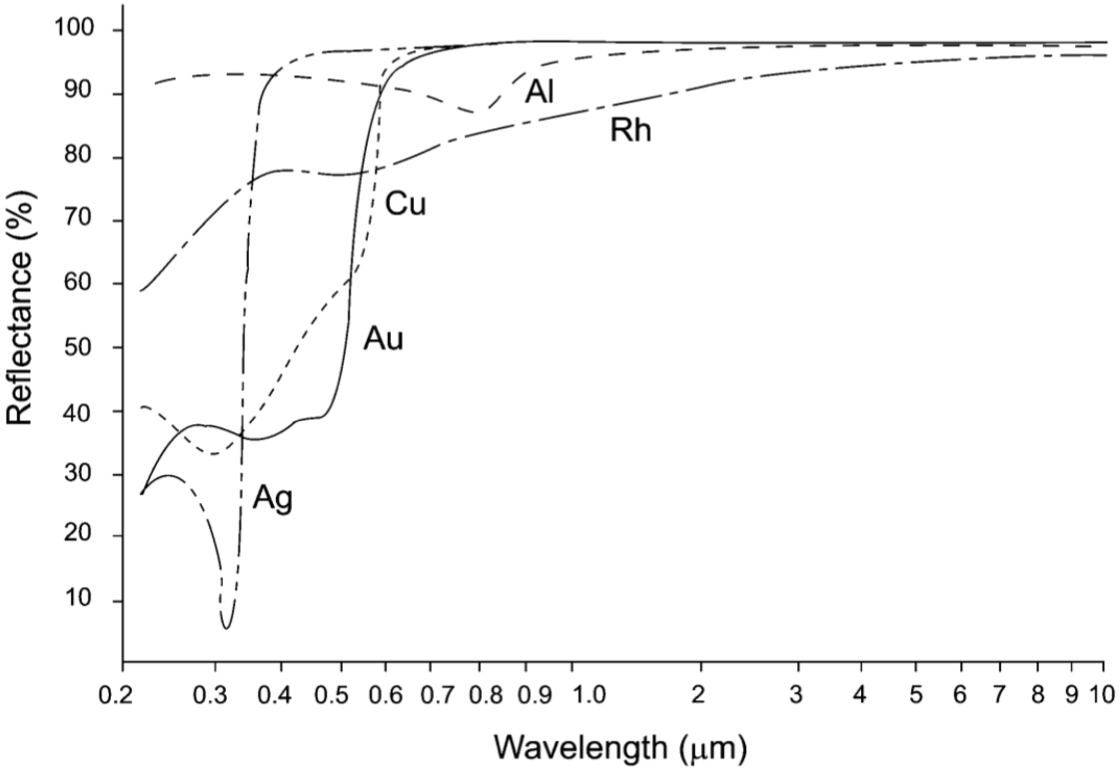

Figure 6.2: Reflectance of thin films of aluminium, copper, gold, rhodium and silver as a function of wavelength from 0.2–10 μm [58].

Metals have a complex index of reflection of the form $N=n\text{-}iK$, where n is the real part of the refractive index, and it is the ratio of the speed of light in a given medium to that in vacuum, K is the imaginary part of the complex refractive index, and it is related to the absorption of light by the medium.

The electromagnetic wave propagating in a metal in the z direction can be expressed as:

$$E(z) = E_0 e^{(-iNkz)} = E_0 e^{(-inkz)} e^{(-ikKz)} \quad where \quad k = \left(2\pi/\lambda\right)$$

$$E(z) = E_0 e^{\left(-\frac{2\pi Nz}{\lambda}\right)} = E_0 e^{\left(-i\frac{2\pi nz}{\lambda}\right)} e^{\left(-\frac{2\pi Kz}{\lambda}\right)} \qquad (5)$$

Equation five consists of two terms the first term describes a non-decaying wave amplitude, where is the second term reflects how the wave amplitude decreases exponentially as a function of z in the metal film, we call this term the damping factor.

Then the fraction of the electromagnetic wave that has propagated through the material can be expressed by

$$E(z) = E_0 e^{(-\alpha z)} = E_0 e^{\left(\frac{-2\pi k}{\lambda} z\right)}.$$

And the distance where the amplitude of the electromagnetic field *E (z)* decreases to $E(z) = E_0 e^{(-1)}$, is called the skin depth and it is given by equation (6) [55,59]:

$$\delta = \frac{1}{\alpha} = \frac{\lambda}{2\pi k} \qquad (6).$$

Therefore the thickness of metallic thin film mirror can effect the transmission of light and consequently the performance of the optical filter.

Figure 3 below shows the k value of aluminum, and figure 4 shows the transmission and reflectance of aluminum as they vary with thickness at λ= 2 um. The skin depth of aluminum at 2 um is:

$$\delta = \frac{1}{\alpha} = \frac{\lambda}{2\pi k} = \frac{2e^{-6}}{2 * \pi * (20.3)} = 15.7nm$$

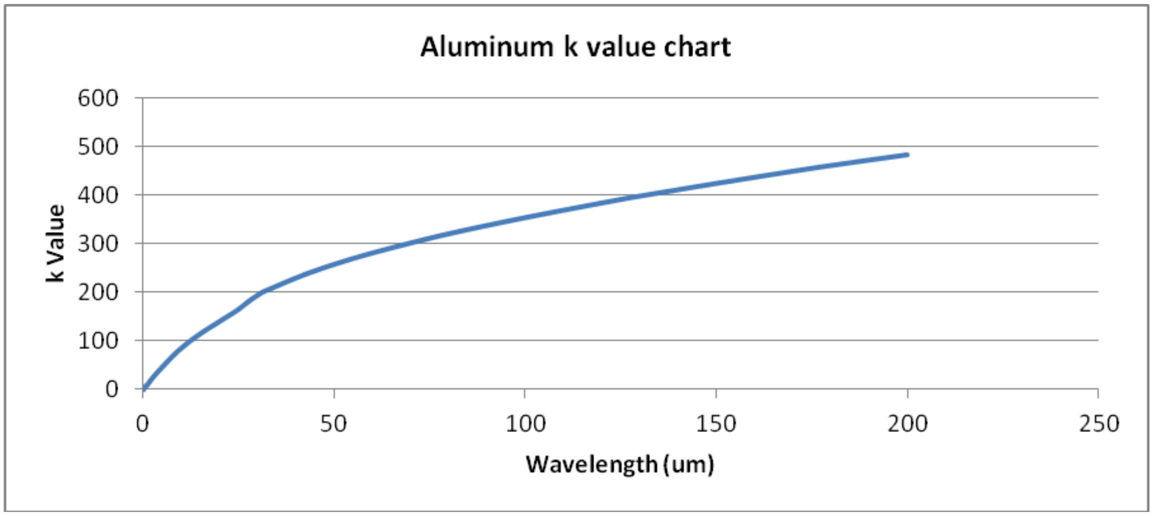

Figure 6.3: K value of aluminium [60].

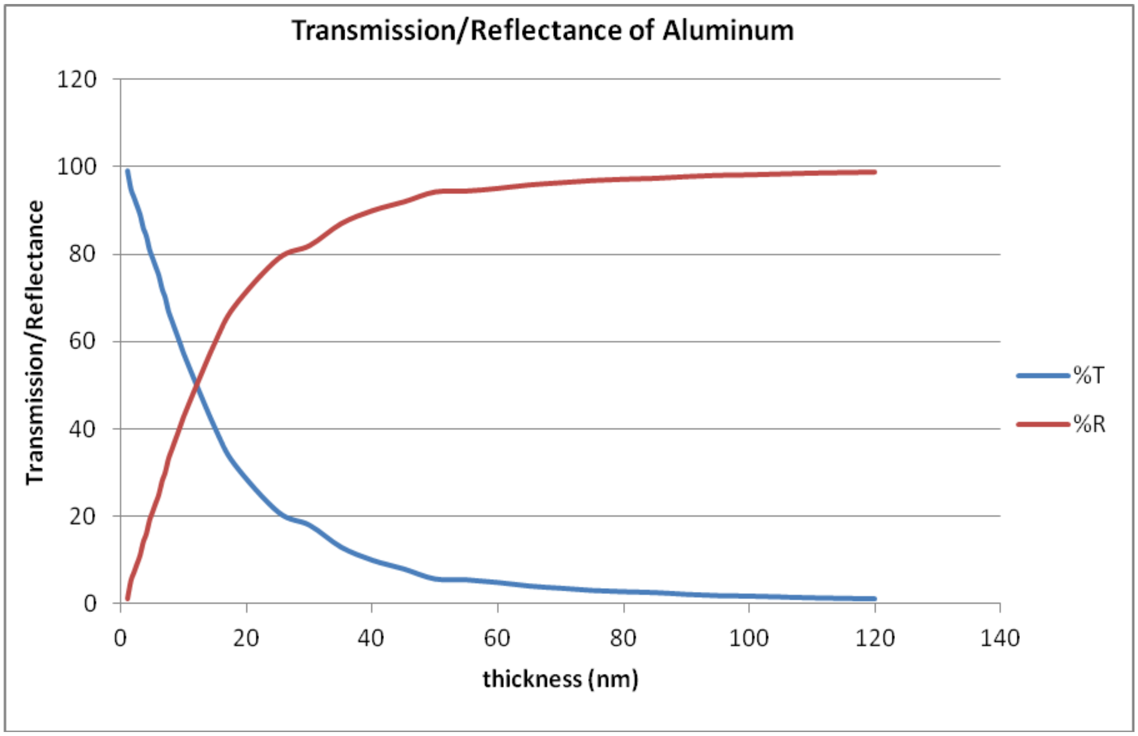

Figure 6.4: Transmission and reflectance of aluminum as a function of film thickness

6.3.1 Dielectric Mirrors

Dielectric mirrors consist of stacking alternating layers of dielectric materials of low and high reflective indices. The high reflectance is achieved due to the fact that when the light beams reflect at the interfaces of the different layers, they all reach the front surface having the same phase shift, which allows them to interface constructively.

This stack of dielectric layers is also called Distributed Bragg Reflector.

For a given wavelength, the reflectance in air for this stack of layer is given by [58]:

$$R = \left(\frac{1 - (n_H / n_L)^{2p} (n_H^2 / n_S)}{1 + (n_H / n_L)^{2p} (n_H^2 / n_S)} \right)^2 \qquad (5)$$

Where n_H, n_L, and n_S are the indices of refractive of the high index, low index and the substrate layers respectively, p is the pairs of high/low-index layers.

The relationship between reflectivity and the number of stack layers is depicted in figure (5) below.

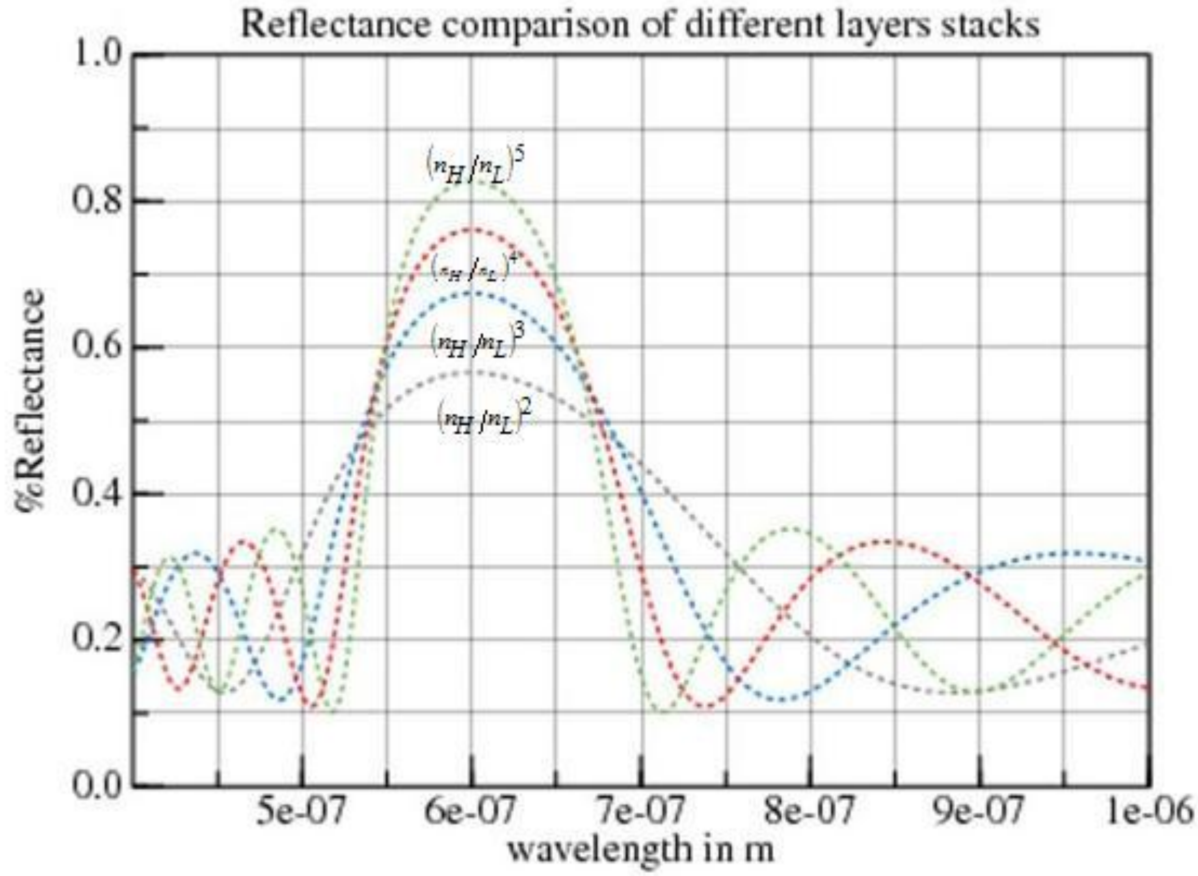

Figure 6.5: Reflectance with different number of stack layers.

Dielectric mirrors are characterized by their robustness, low maintenance, and low absorption loss [58].

CHAPTER VII: FILTER DESIGN AND FABRICATION

7.1 Filter Design

Since the glucose wavelengths of interest are in the 7 to 10 µm ranget, the Fabry-Perot filters were designed to resonate at the mid-infrared spectrum. The mirrors were designed for central wavelength of 9.2 µm, with the ability to be tuned at 8.4 µm and 10.1 µm.

Table 1 below summarises the design parameters of the filter. Where m is the order number, λ_m is the center wavelength, and is the distance between mirrors.

Table 7.1. Design parameters

<table>
<tr><td></td><td>1 (um)</td><td colspan="2">3 (um)</td><td>4 (um)</td></tr>
<tr><td>λ_c</td><td>8.4</td><td colspan="2">9.2</td><td>10.1</td></tr>
<tr><td>λ/m</td><td>8.4</td><td colspan="2">9.2</td><td>10.1</td></tr>
<tr><td colspan="5">Design Parameters (m=1)</td></tr>
<tr><td>Value</td><td colspan="2">d/m</td><td colspan="2">d (um)</td></tr>
<tr><td>1</td><td colspan="2">4.2</td><td colspan="2">4.2</td></tr>
<tr><td>2</td><td colspan="2">4.5</td><td colspan="2">4.5</td></tr>
<tr><td>3</td><td colspan="2">5.05</td><td colspan="2">5.05</td></tr>
</table>

7.1.1 Dielectric Mirror Design

The dielectric mirros design is based on the Bragg reflector structure which consists of alternating quarter wave optical thickness (QWOT) layers with low and high refractive index. In order to build high reflective mirrors in the desired wavelength range, without stacking too many layers of thin films, the refractive index ratio n_H/n_L has to be as high as possible.

Potential thin films to be used as a low refractive index material are zinc oxide (ZnO) or zinc sulfide (ZnS) and germanium (Ge) as high refractive index material. The refractive index n of Ge, ZnS, and ZnO are show in figures 6,7, and 8 respectively [60].

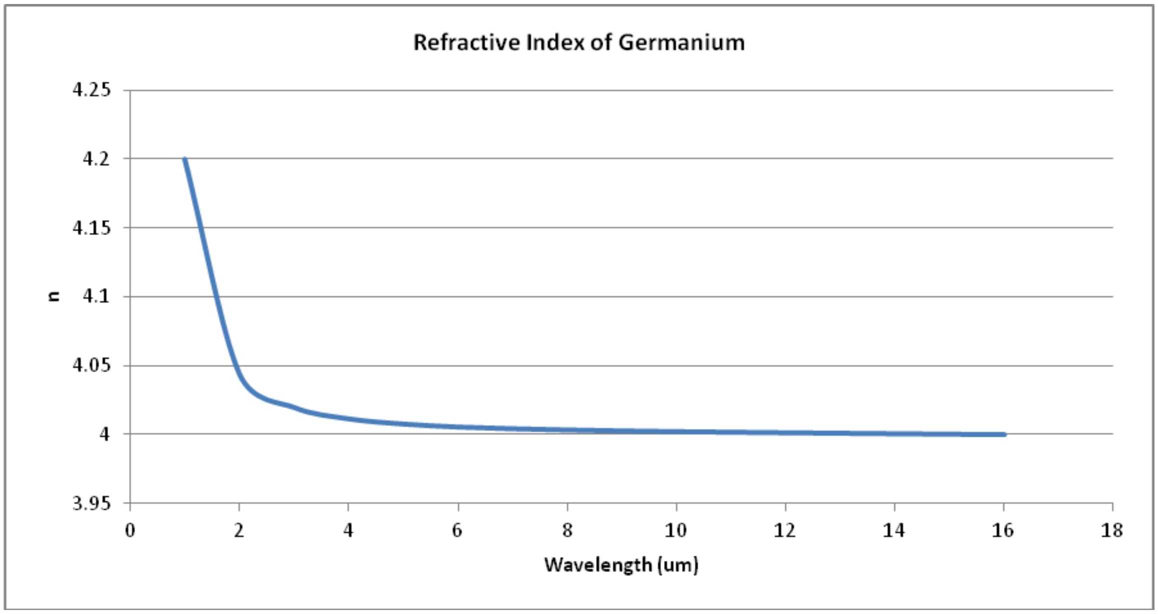

Figure 7.1: Refractive index of Germanium [60].

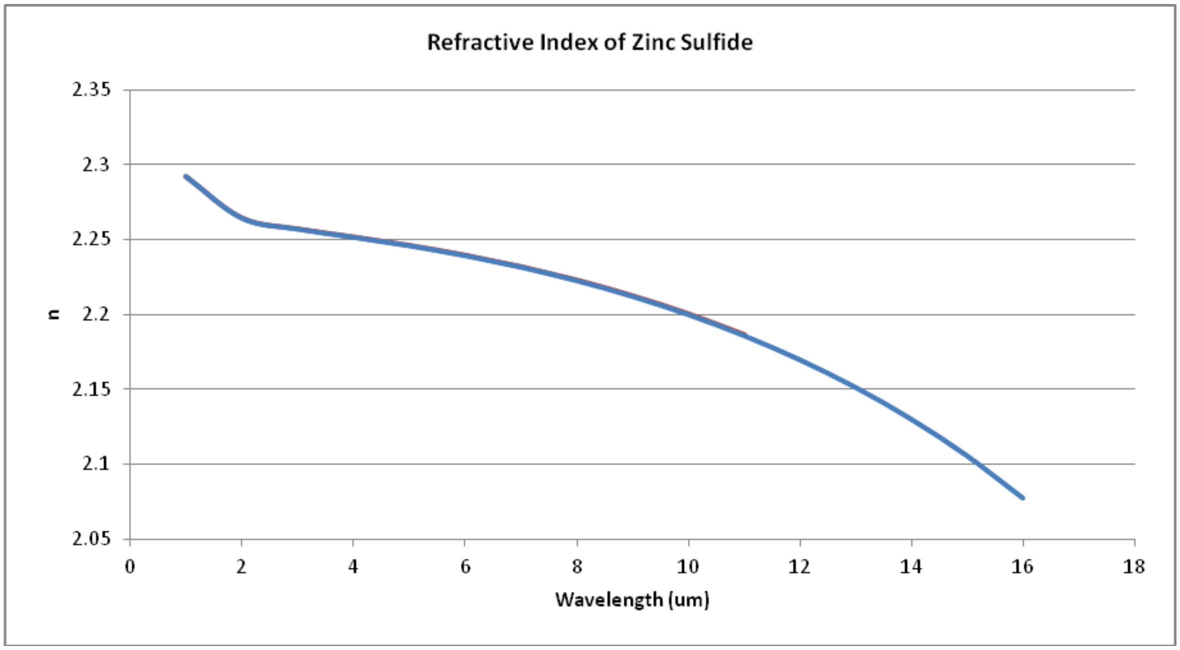

Figure 7.2: Refractive index of Zinc Sulfide [60].

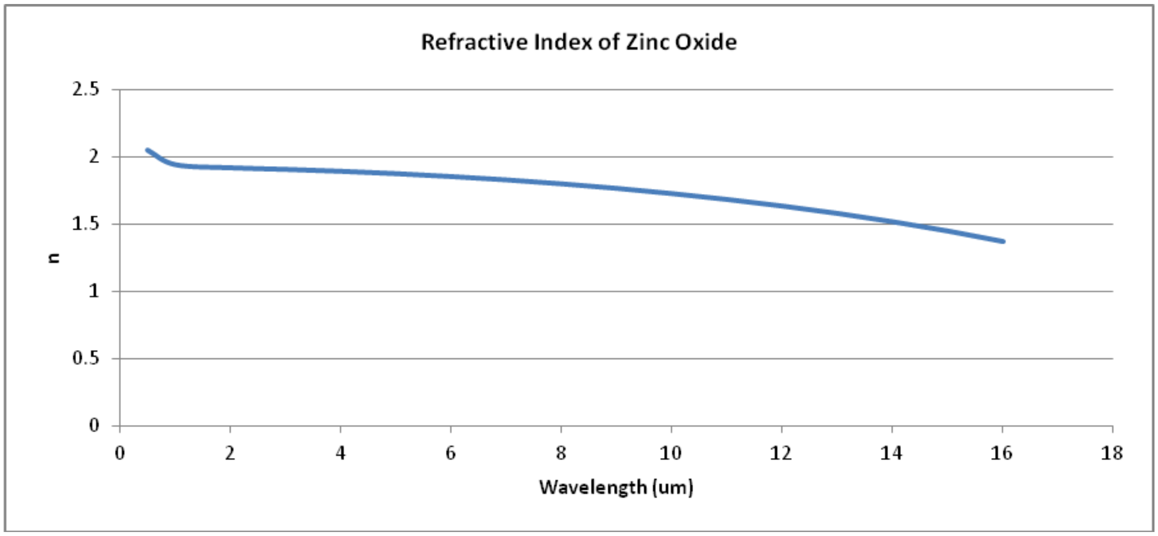

Figure 7.3: Refractive index of Zinc Oxide [60].

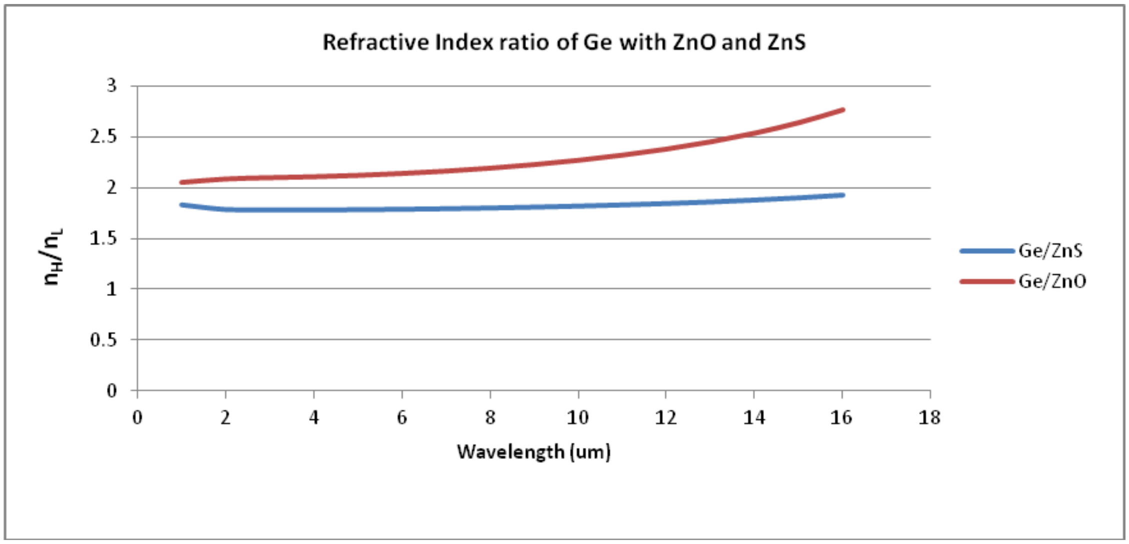

Figure 7.4: Refractive index ratio of Ge/ZnO and Ge/ZnS

Based on the plot of figure 9, the Ge/ZnO ration will give us higher reflectivity than the Ge/ZnS ratio.

The ZnO layer is deposited by sputtering process and the Ge layer was deposited by the e-beam process.

The layers thickness (d) was calculated according to the quarter wave optical thickness method:

$$d = \frac{\lambda_c}{4n} \qquad (6)$$

Where λ is the center wavelength, *n* is the refractive index of the material, and *d* is the layer thickness.

7.1.2 Mechanical Design

The Fabry-Perot interferometer is designed with two fixed mirrors separated by a distance d. Each mirror consists of a stack of alternating layers of dielectric materials, Ge as a high index material, and ZnO as a low index material. The layers are deposited on a 300 μm thick silicon substrate as illustrated in figure 10 below.

Figure10. Mirror structure.

🟦 Ge layer

⁘ ZnO layer

🟦 Si substrate

7.1.3 Fabrication

Step 1. SiO_2 layer growth

Step 2. Apply photo-resist

Step 3. Apply pattern and expose to UV Light

Step 4. Strip photo-resist

Step 5. Remove the SiO_2

Step 6. Etch of Si wafer

Step 7. Strip photo-resist and SiO_2

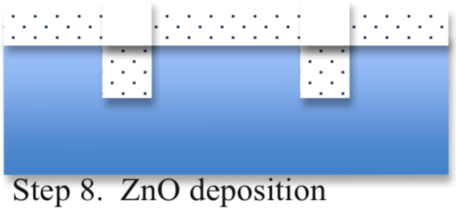

Step 8. ZnO deposition

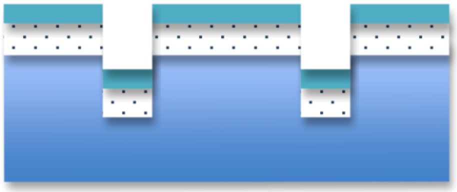

Step 9. Ge deposition

The silicon wafer must be clean of any contamination at all the fabrication stages. The wafer was first cleaned in a 2-3 solution of Hydrogen Peroxide (H_2O_2) and Sulfuric acid (H_2SO_4) to remove any organic and metallic materials. After that the wafer was rinsed in de-ionized (DI) water for 5 minutes. Then the wafer was dipped in a 10% Hydrofluoric Acid (HF) for 10 seconds, to remove any oxide impurities from the wafer.

Step 1. Oxidation Process

A dry and wet oxidation processes used to grow the SiO_2 layer on the silicon wafer as follows:

1- $Si + N_2 + O_2 \longrightarrow SiO_2 + N_2$ (5 minutes, dry)

2- $Si + N2 + 2H_2 + 2O_2 \longrightarrow SiO_2 + 2H_2O + N_2$ (40 minutes, wet)

3- $Si + N_2 + O_2 \longrightarrow SiO_2 + N_2$ (5 minutes, dry)

Step 2. Apply Photoresist

A blob of positive photoresist (Microposit 1813) is applied on the wafer and then spun for 60 seconds at 4000 rpm, to give an evenly spread layer of photoresist. The wafer is then soft-baked on a hot plate (115 C) for 60 seconds, which allows for better adhesion of the photoresist to the silicon wafer.

Step 3. Apply pattern and expose to UV Light

Align the mask/pattern on the silicon wafer, then expose to Ultra-Violet (UV) light for 40 seconds. This process allows the exposed photoresist to develop in the photoresist developer.

Step 4. Strip photo-resist

After exposure to UV light, submerse the silicon wafer in the photoresist developer solution to wash away the exposed photoresist and copy the mask pattern to the silicon wafer.

Step 5. Remove the SiO_2

To remove the SiO_2 layer, the wafer was submersed in a 10% HF for 20 seconds, then rinsed in DI water for 10 seconds.

Step 6. Etch of Si wafer

The silicon was etched in a 45% Potassium hydroxide (KOH) at 70 C for 3 to 5 minutes to get the required etch thickness.

Step 7. Strip photo-resist and SiO_2

After etching the Si it was time to remove the photoresist and the SiO_2.
The photoresist was stripped by submersing the wafer in Acetone for 5 minutes, then Methanol for 5 minutes, and finally rinsing in DI water for 5 minutes and then drying with nitrogen.

The SiO_2 was removed by submersing the wafer in 10% HF for 20 seconds, rinsing in DI water for 10 minutes and then drying with nitrogen.

Step 8. ZnO deposition

The ZnO film was deposited using sputtering deposition technique [72-74]. Sputtering technique is a process by which the Si wafer (or any substrate where the film will be grown) is placed in a vacuum chamber filled with Argon gas. Then a high voltage is applied in the chamber to ionize the gas and create plasma. The Ar^+ ion accelerates towards the target at high speed and knock off atoms from its surface. These atoms hit the substrate and condense as a film.

Step 9. Ge deposition

The Ge thin film was deposited by the E-beam deposition technique. The e-beam or electron beam evaporation process is an evaporation deposition technique where the substarte is placed in a vacuum chamber and the material to be deposited is a placed in graphite crucible. Inside the chamber there is a tungsten filament that is heated and when it gets too hot it starts emiting electrons. These electrons are deflected and focused on the material to be evaporated. Upon hitting the material, the electrons heat it up and cause it to evaporate and deposit on the substrate.

CHAPTER VIII: TEST AND MEASUREMENT

8.1 Layers Measurement

The layers thicknesses were measured using a Scanning Electron Microscope (SEM) to determine the exact thickness of the ZnO and the Ge layers.

8.1.1 Scanning Electron Microscope (SEM)

SEM stands for Scanning Electron Microscope. SEM is different from a typical light microscope by the fact that it uses high energy electron beam instead of light which allows for much higher magnification.

The main components of an SEM are Electron Source, Electron Lenses, vacuum chamber, detectors, signal processor, and a display.

The electron source maintains a stream of high electron beam shooting at the sample under test, the electron lenses are made of magnets and they are used to control the electrons and make sure they are focused on the sample [77-82].

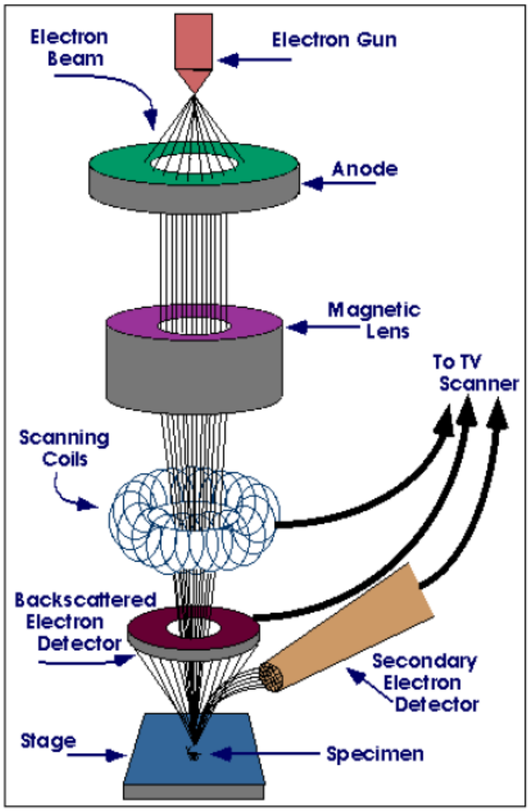

Figure 8.1: Schematic of an SEM [77]

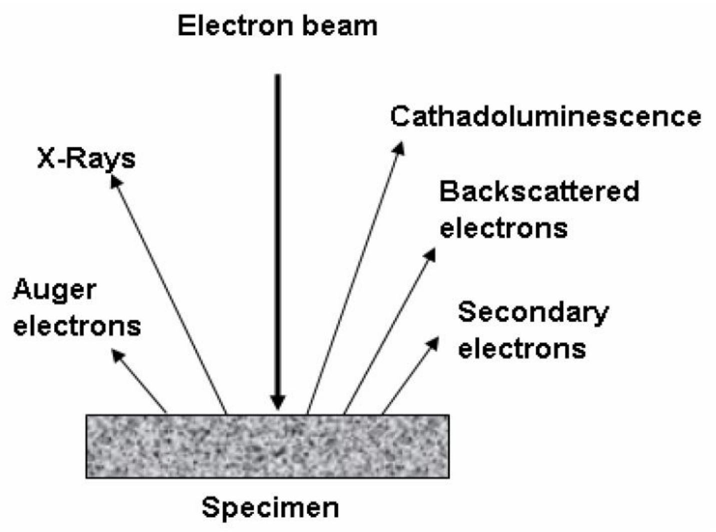

Figure 8.2: Generated signals after the interaction of electrons with the sample atoms [78].

Upon impinging on the sample the electrons interacts with the atoms of the sample, resulting in multiple signals: backscattered electrons, secondary electrons, X-Rays, Auger electrons, cathadoluminescence.

These signals are then captured by the corresponding detectors, processed by the signal processor and displayed for interpretation [77-82].

8.1.2 Layers Thicknesses

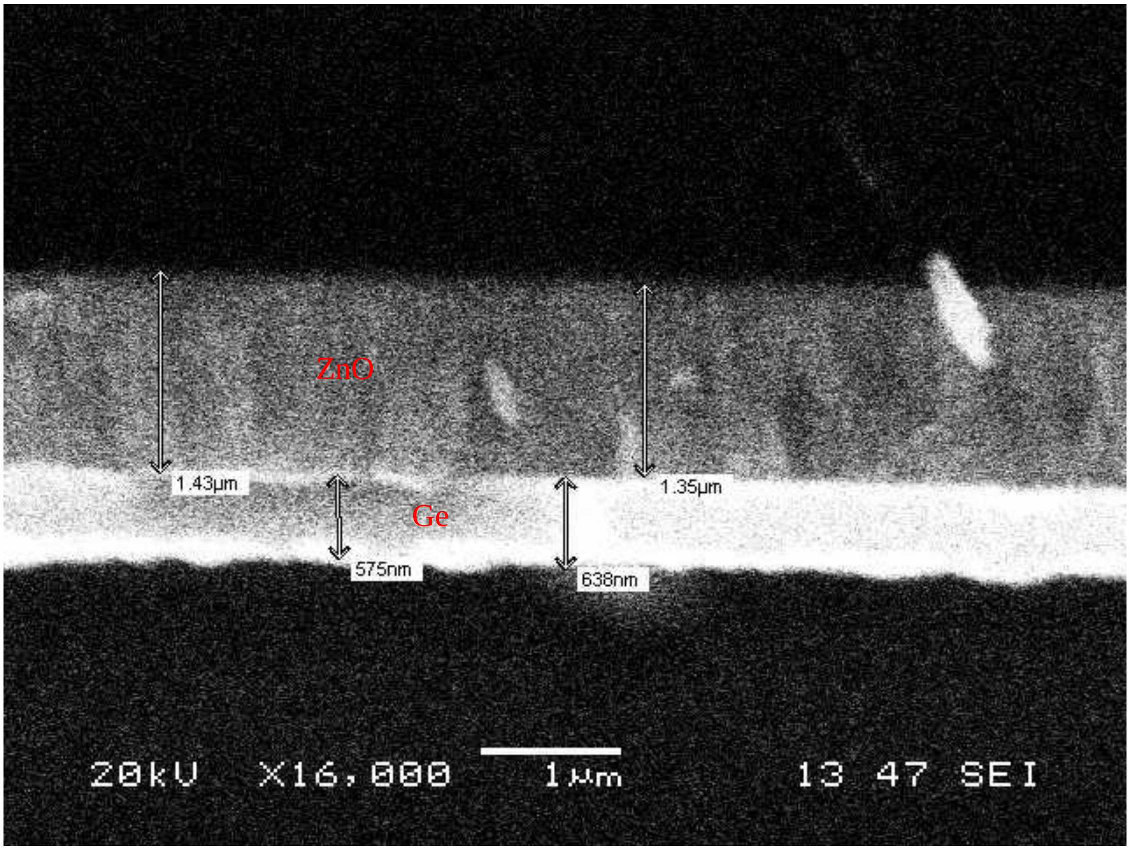

Figure 8.3: The thicknesses of ZnO and Ge layers measured by SEM.

Based on figure 7.3 the layer were not uniformely grown, in the case of ZnO the thickness was within 200 nm of the calculated value and the Ge layer within 60 nm of the calculated value.

8.2 Simulation and Test results

The fabricated FP filter is tested using Fourrier-Transform Infra-Red Spectroscopy (FTIR), and the result then compared with the simulated data.

8.2.1 FTIR Spectroscopy

FT-IR spectrometer consists of an IR source, mirrors, interferometer, detector, and a signal processor. The interferometer is, typically, a Michelson interferometer which is composed of a beam splitter, a fixed mirror, and a movable mirror. Figure 1 below shows a typical layout of a spectrometer.

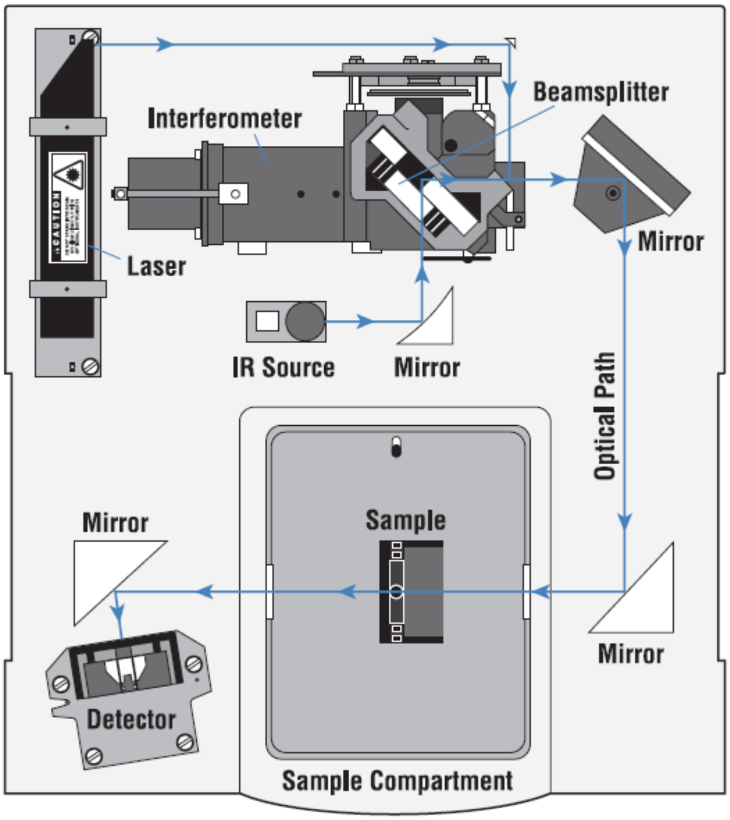

Figure 8.4: Typical spectrometer layout [83].

The IR source shines on the interferometer where the incoming IR beam splits by the beam splitter to produce two beams. One beam reflects off a fixed mirror with a fixed distance back to the splitter and the other beam reflects off a movable mirror with a variable distance back to the splitter [83,84].

Both beams meet at the beam splitter where they interfere destructively or constructively and the resulting signal is called interferogram [83,84].

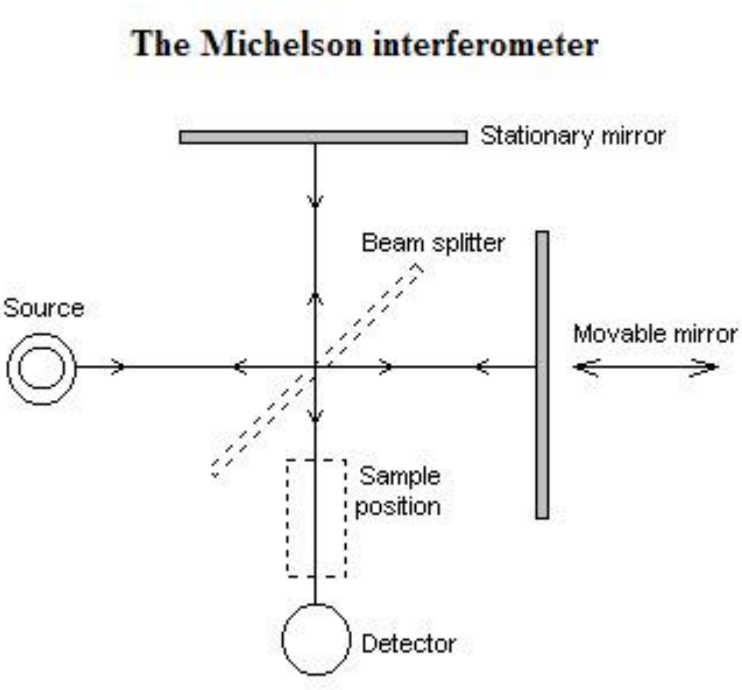

Figure 8.5: Michelson Interferometer schematic [84]

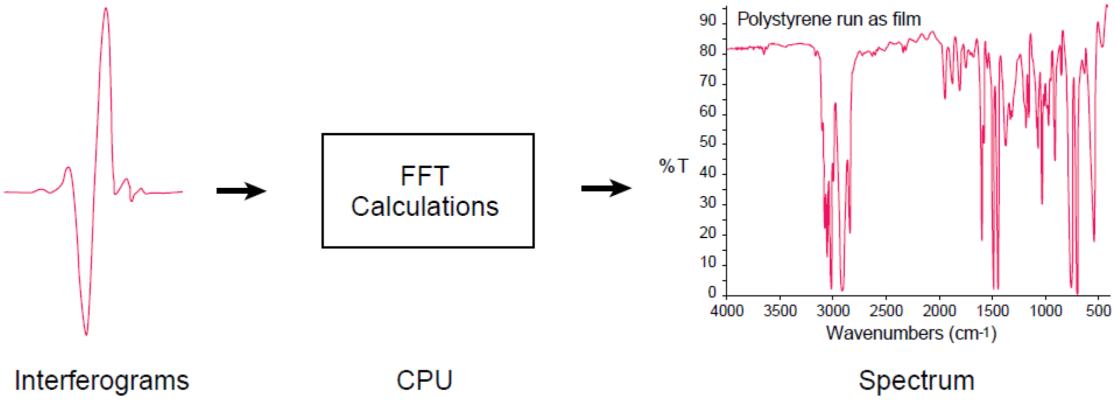

Figure 8.6: An interferogram signal and the resulting spectra after FFT analysis [84].

The interferogram, which contains different frequencies, passes through the sample which absorbs or transmits at specific frequencies and finally to the detector to measure the signal. After that the signal processor analyses the detected signal using Fourier Transform and plots the spectral characteristics for analysis.

8.2.2 Results

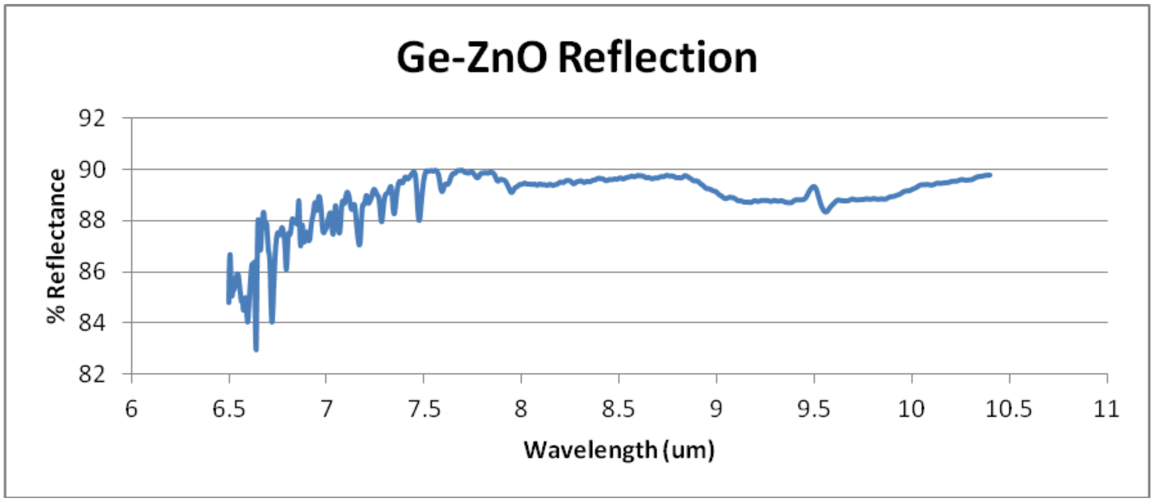

Figure 8.7: Ge/ZnO (on a Si substrate) reflection spectra measured using FTIR spectroscopy.

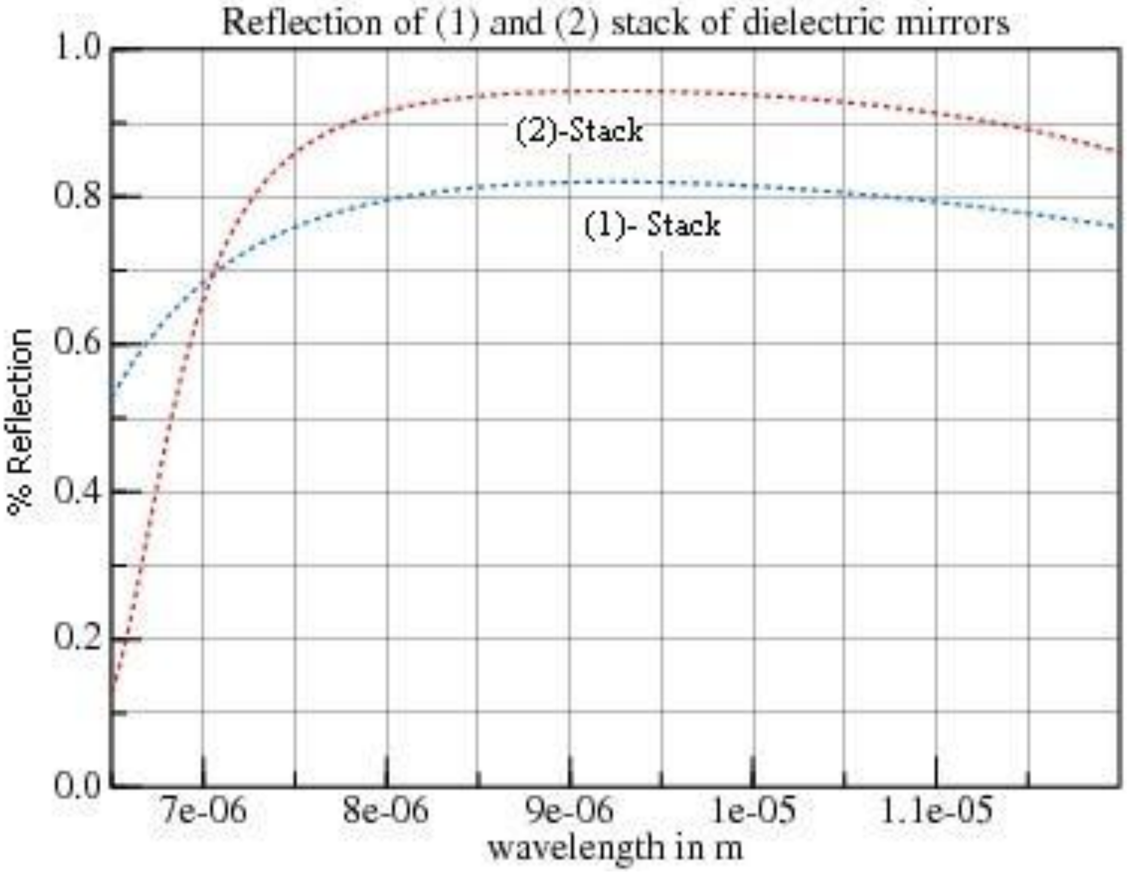

Figure 8.8: Simulated reflection of Ge/ZnO on Si substrate. Simulation performed using Freesnell Software.

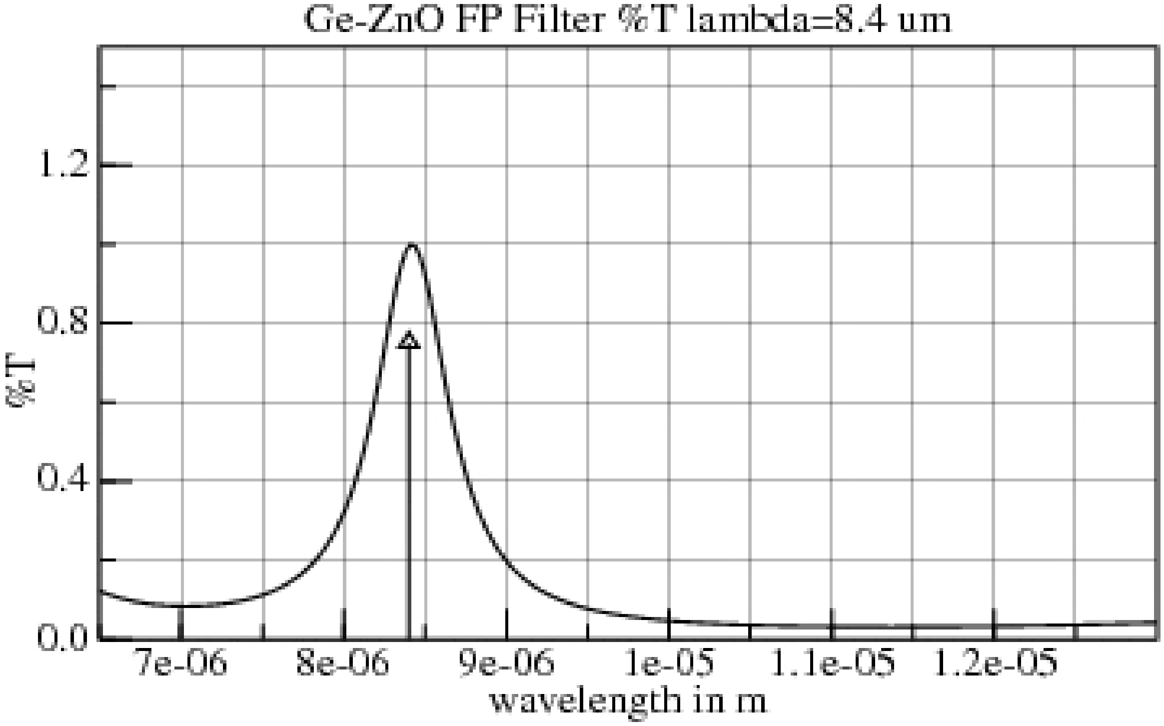

Figure 8.9: Simulated FP filter with seperation air distance between mirror d_{air} = 4.2 μm. With this distance, the filter resonates at wavelenthg λ= 8.4 μm. Simulation performed using Freesnell Software.

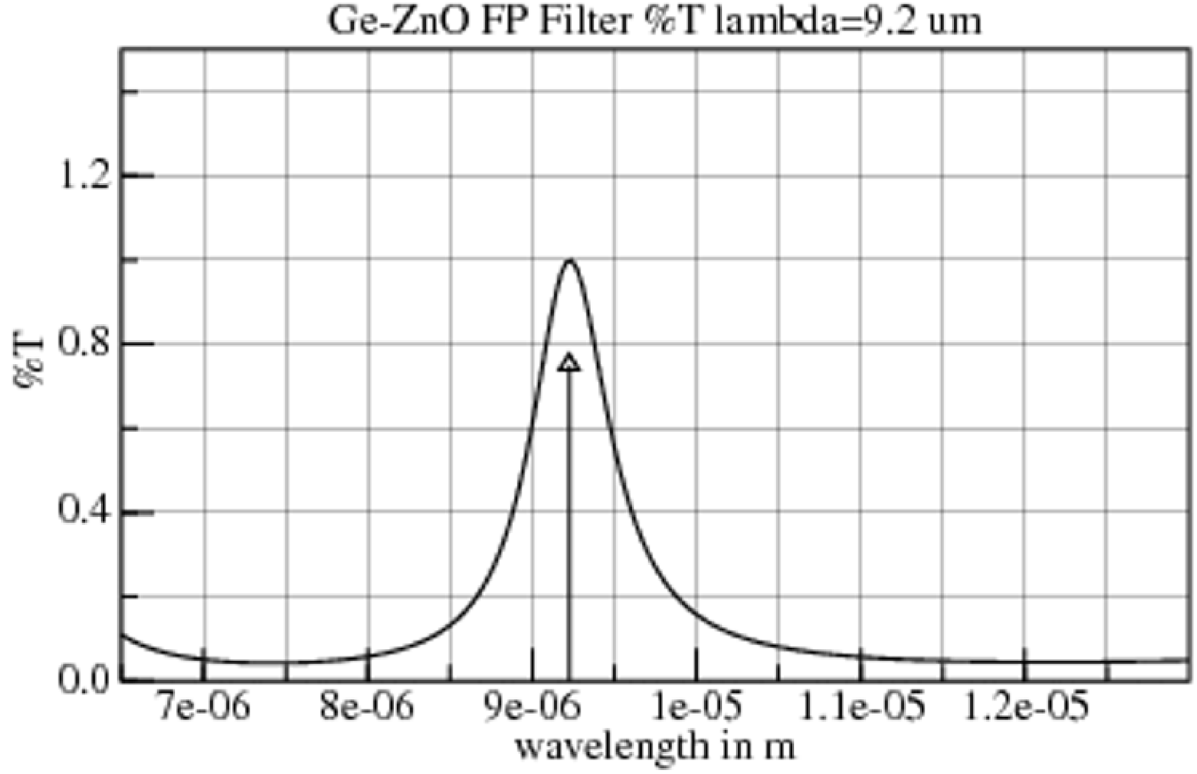

Figure 8.10: Simulated FP filter with seperation air distance between mirror d_{air} = 4.5 μm. With this distance, the filter resonates at wavelenthg λ= 9.2 μm. Simulation performed using Freesnell Software.

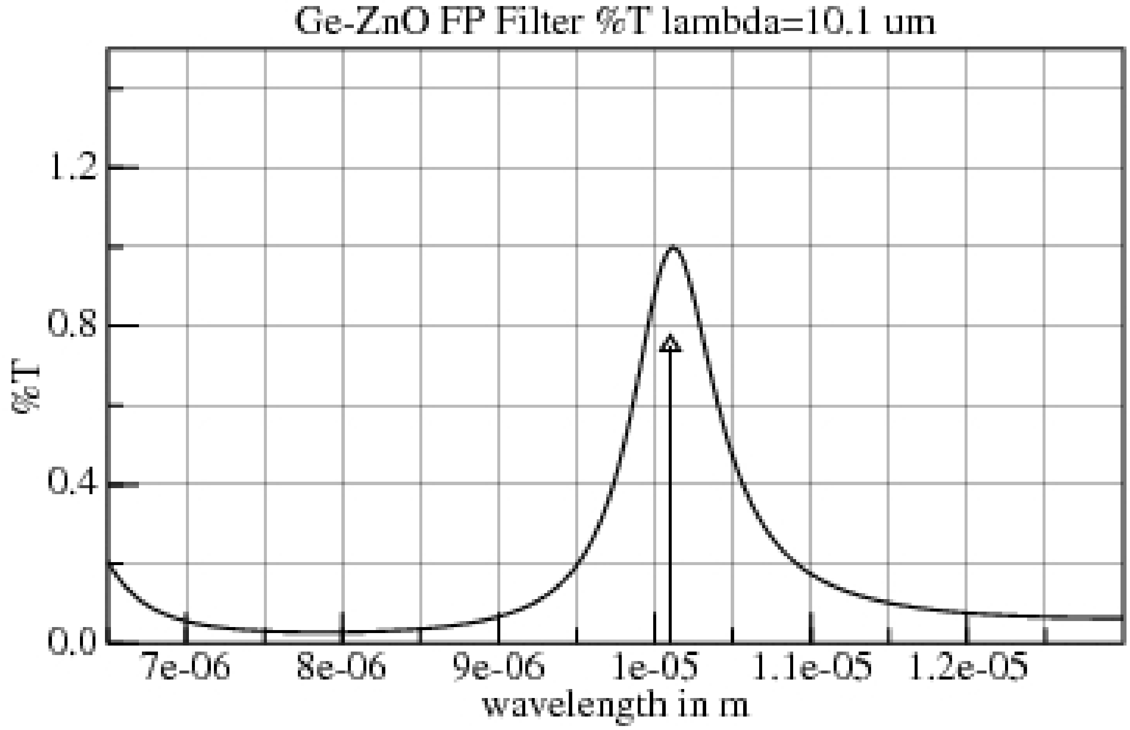

Figure 8.11: Simulated FP filter with seperation air distance between mirror d_{air} = 5.05 μm. With this distance, the filter resonates at wavelenthg and λ= 10.1 μm. Simulation performed using Freesnell Software.

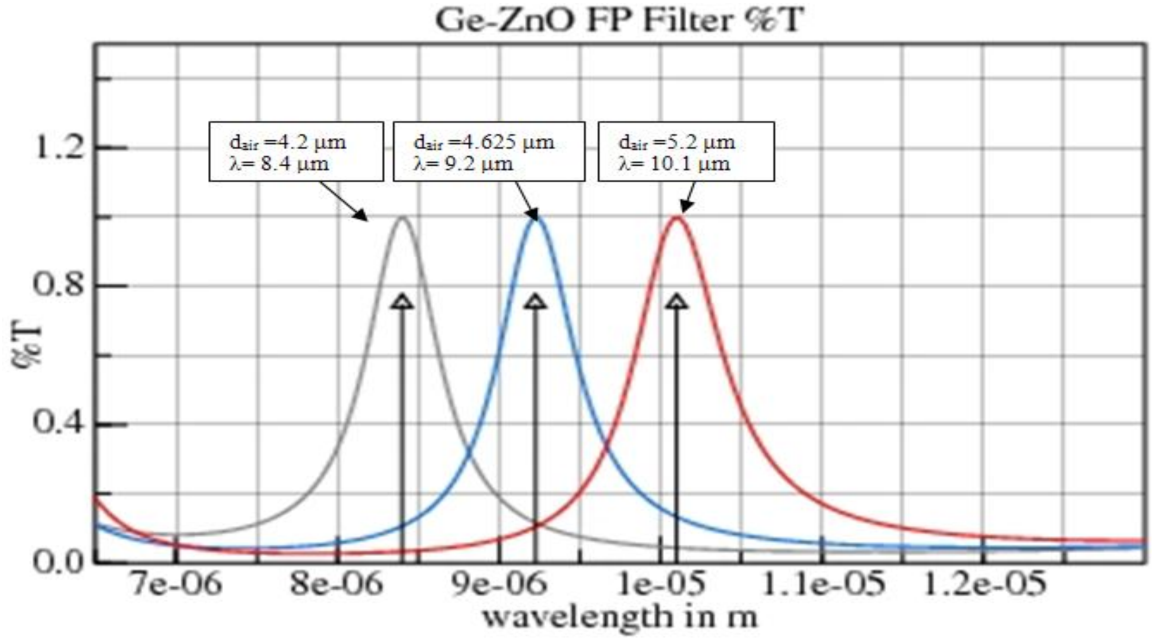

Figure 8.12: Simulated FP filter with all three different distances d_{air} between the mirrors. The corresponding resonant wavelength of each distance is plotted as well.

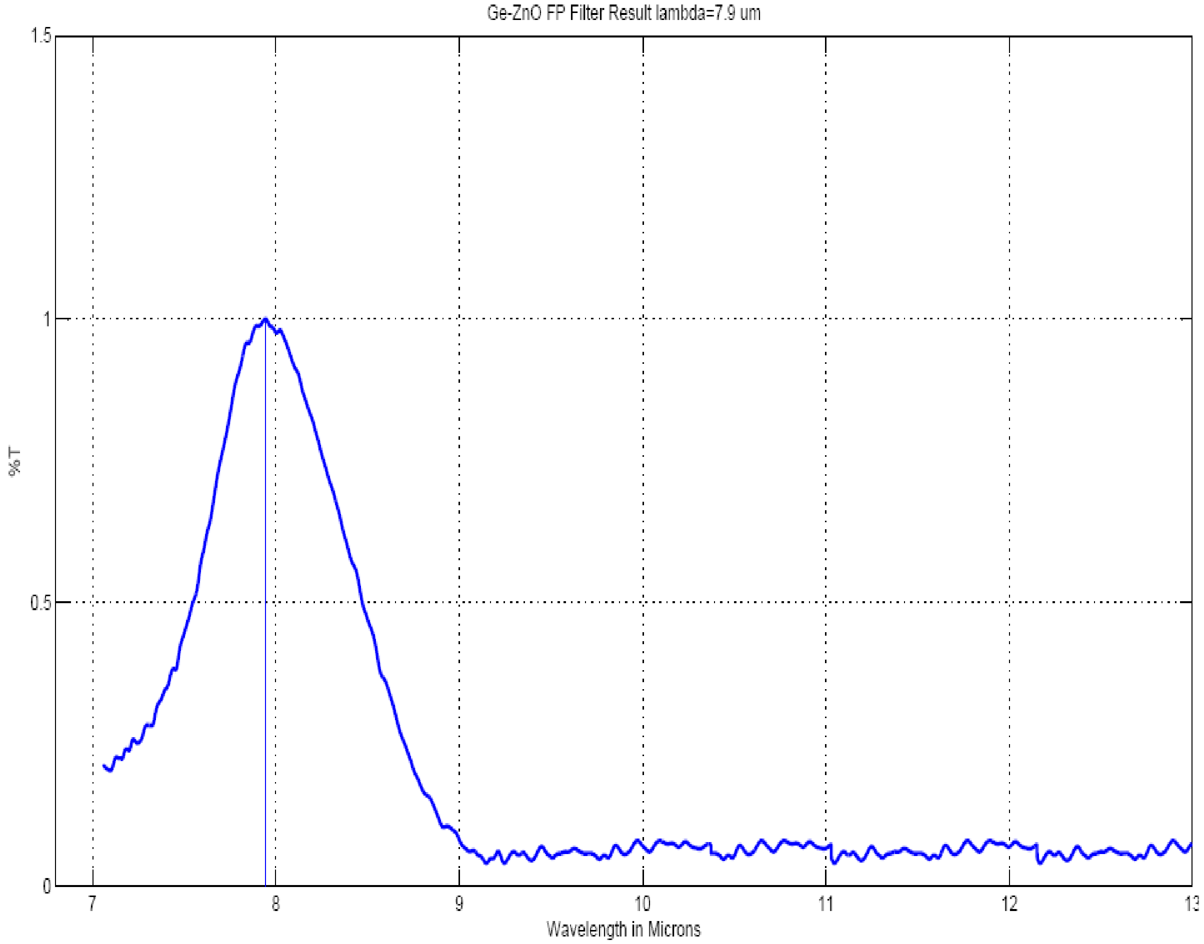

Figure 8.13: Designed FP filter result with seperation distance between mirrors d_{air}= 4.38 μm and the corresponding resonant wavelength λ= 7.9 μm.

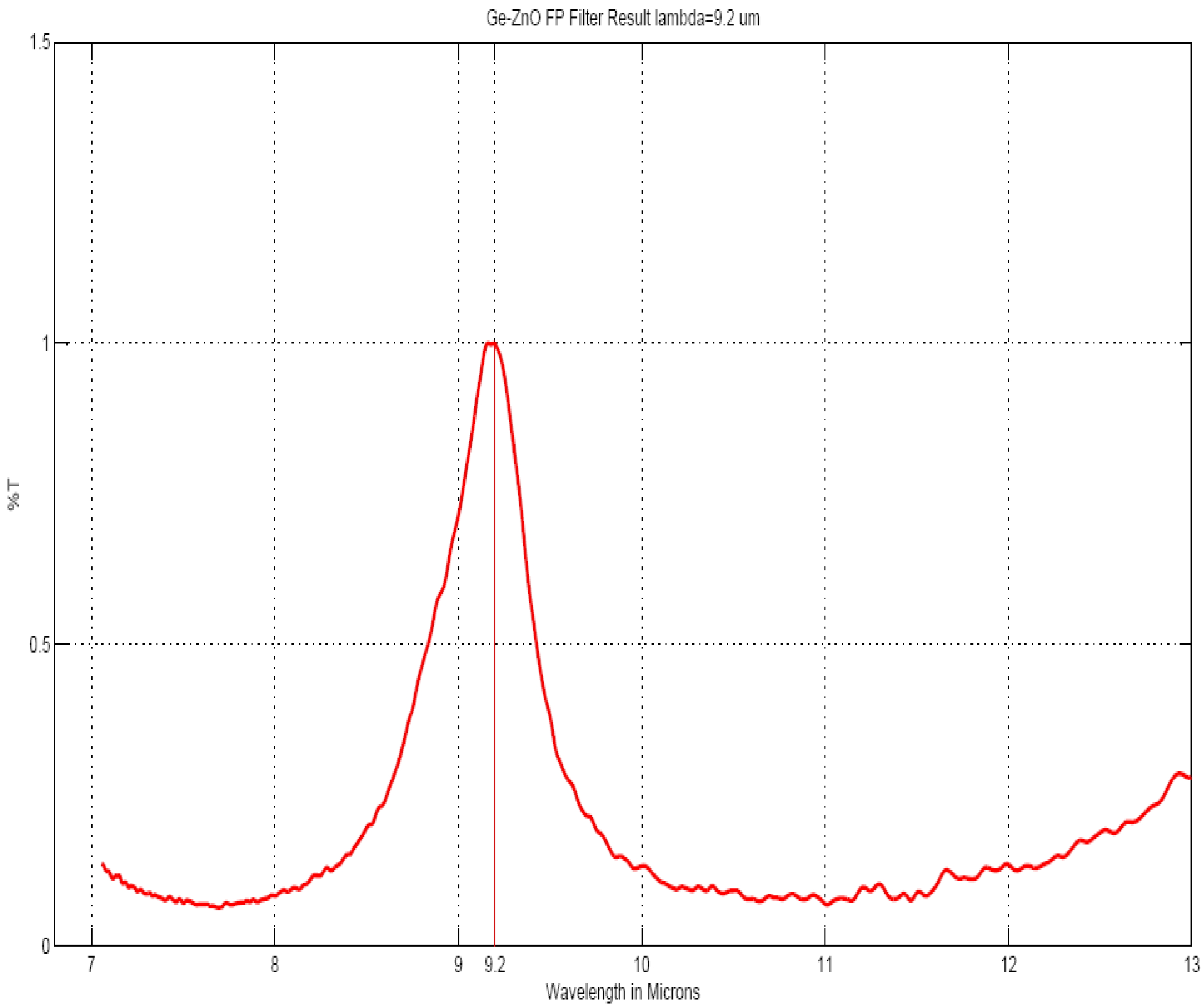

Figure 8.14: Designed FP filter result with seperation distance between mirrors d_{air}= 4.77 μm and the corresponding resonant wavelength λ= 9.2μm.

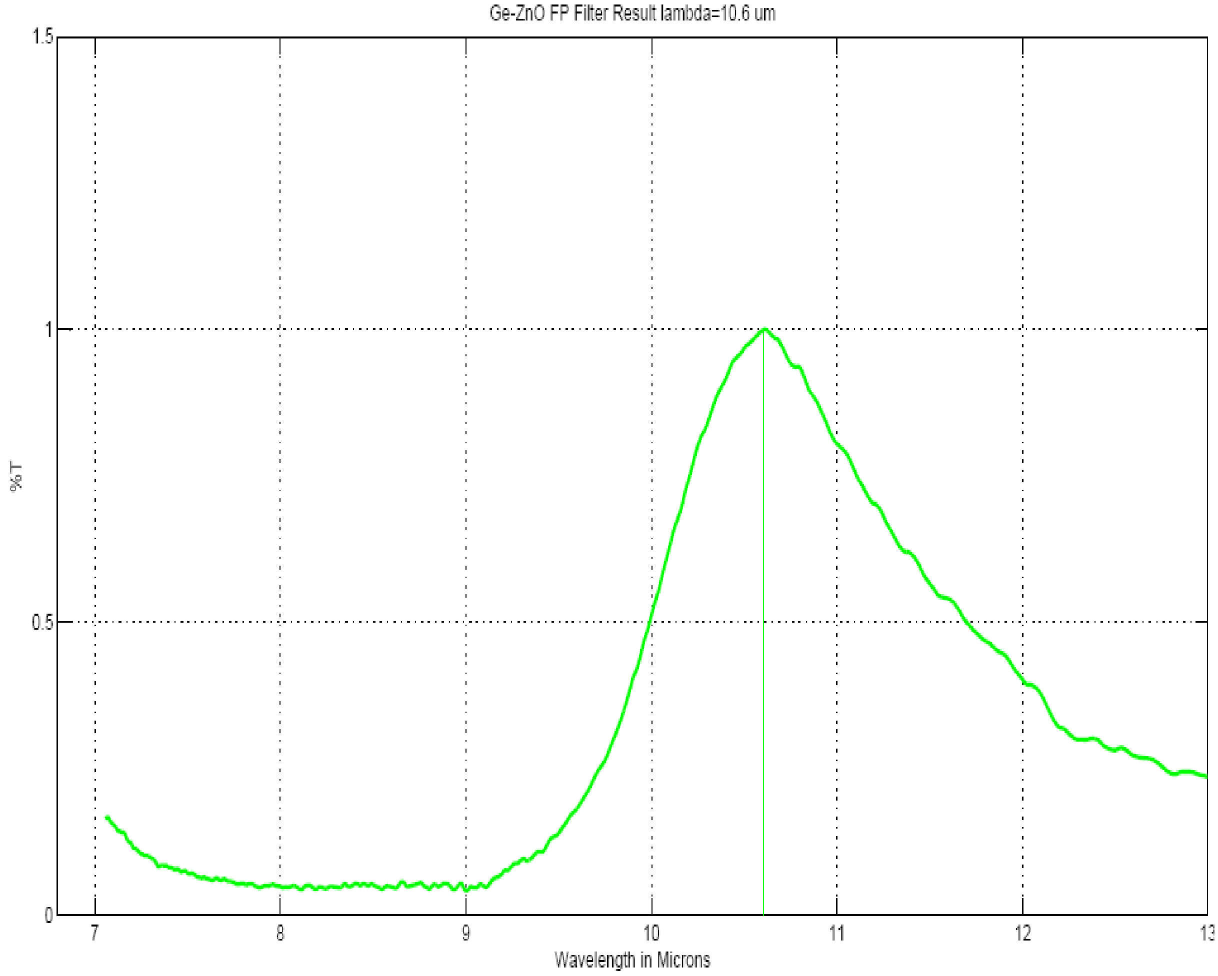

Figure 8.15: Designed FP filter result with seperation distance between mirrors d_{air}= 5.4 μm and the corresponding resonant wavelength λ= 10.6 μm.

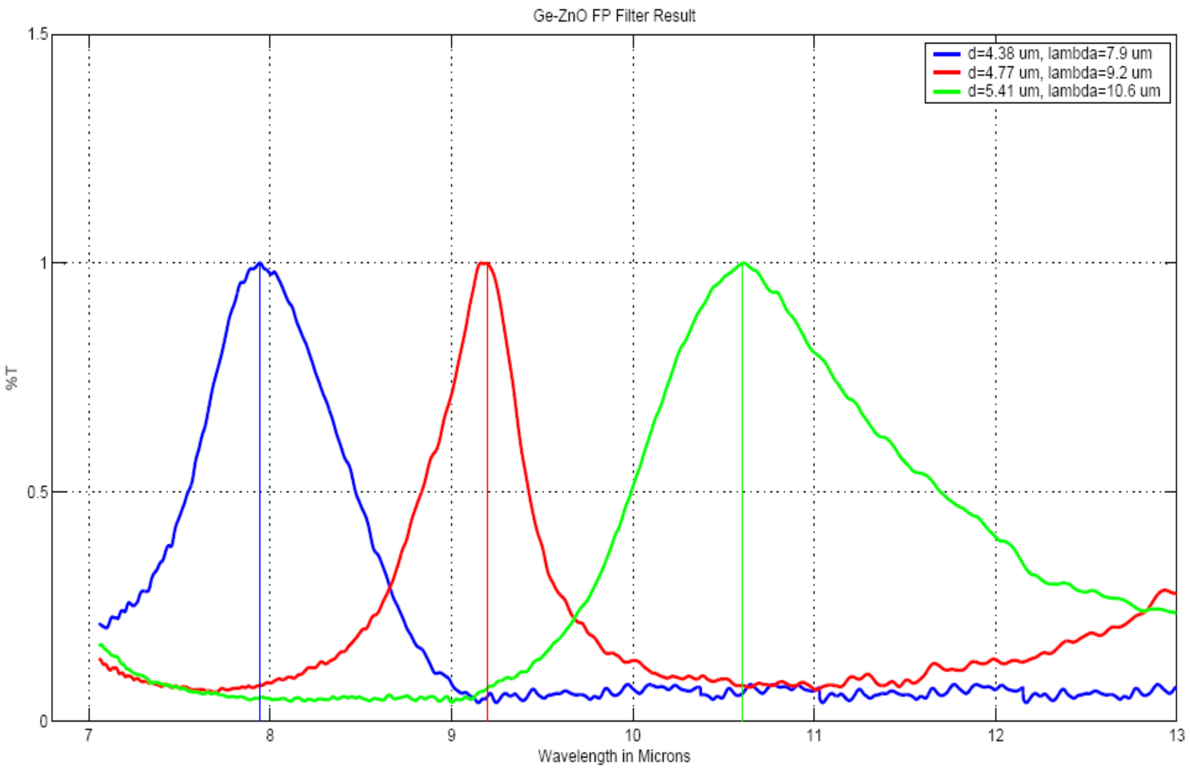

Figure 8.16: Designed Simulated FP filter with all three different distances d_{air} between the mirrors. The corresponding resonant wavelength of each distance is plotted as well.

Table 8.2 below compares the results obtained from simulation and from the final fabry-perot filter design.

Table 8.2. Comparison of the simulation and the final design results

	Design and Simulation comparison					
	FP1		FP2		FP3	
	Simulation	Design	Simulation	Design	Simulation	Design
d_{air}	4.2 mm	4.38 mm	4.6 mm	4.77 mm	5.2 mm	5.41 mm
λc	8.4 mm	7.9 mm	9.2 mm	9.2 mm	10.1 mm	10.6 mm

8.3 Result Analysis

The overall performance of the FPI depends on the finesse $\tilde{F}$ of the filter. The finesse determines the bandpass and the sharpness of the transmitted peak. A high finesse filter results in sharp narrow peaks. However flatness, roughness, and smoothness of the mirror surface affect the optical property of the FPI filter.

The simulation assumes ideal, flat, and smooth mirrors, perfection that is,practically, hard to achieve.

In reality, fabrication imperfections cause deformation of the mirrors surfaces that leads to scattering and consequently reduced reflectivity and finesse [61,62].

The figures below illustrate the effect of roughness on the transmitted peaks.

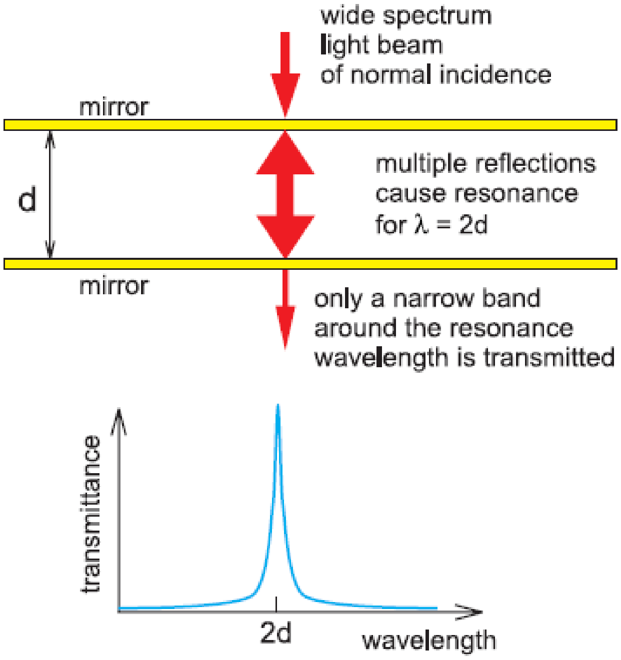

Figure 8.17: Transmission of an ideal Fabry-Perot interferometer [61].

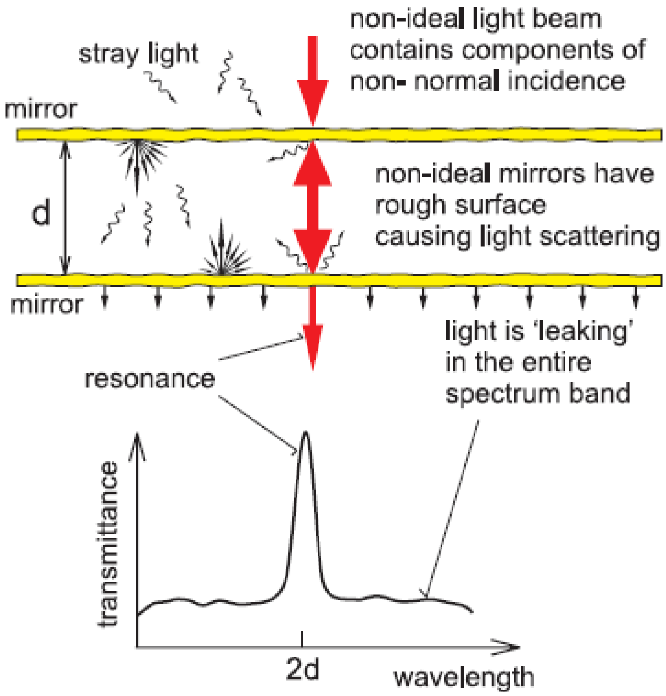

Figure 8.18: Transmission of a non-ideal Fabry-Perot interferometer [61].

Three types of defects could be introduced during the fabrication process, surface roughness δ_{RMS}, surface spherical deviation from plane δ_S, and plate deviation from parallelism δ_P [62,68].

If all three types of defects are considered, then the overall finesse defect F_D for a particular wavelength is given by equation (7) [62,63].

$$\frac{1}{F_D^2} = \left(\frac{2\delta_s}{\lambda}\right)^2 + \left(\frac{4.7\delta_G}{\lambda}\right)^2 + \left(\frac{\sqrt{3}\delta_P}{\lambda}\right)^2 \qquad (7)$$

$$F_D = \frac{\lambda}{\sqrt{\left[4\delta_S^2 + 22.09\delta_{rms}^2 + 3\delta_P^2\right]}} \qquad (7.1)$$

And the effective finesse is given by:

$$F_E = \frac{1}{\sqrt{\left(1/F_R^2\right) + \left(1/F_D^2\right)}} \qquad (8)$$

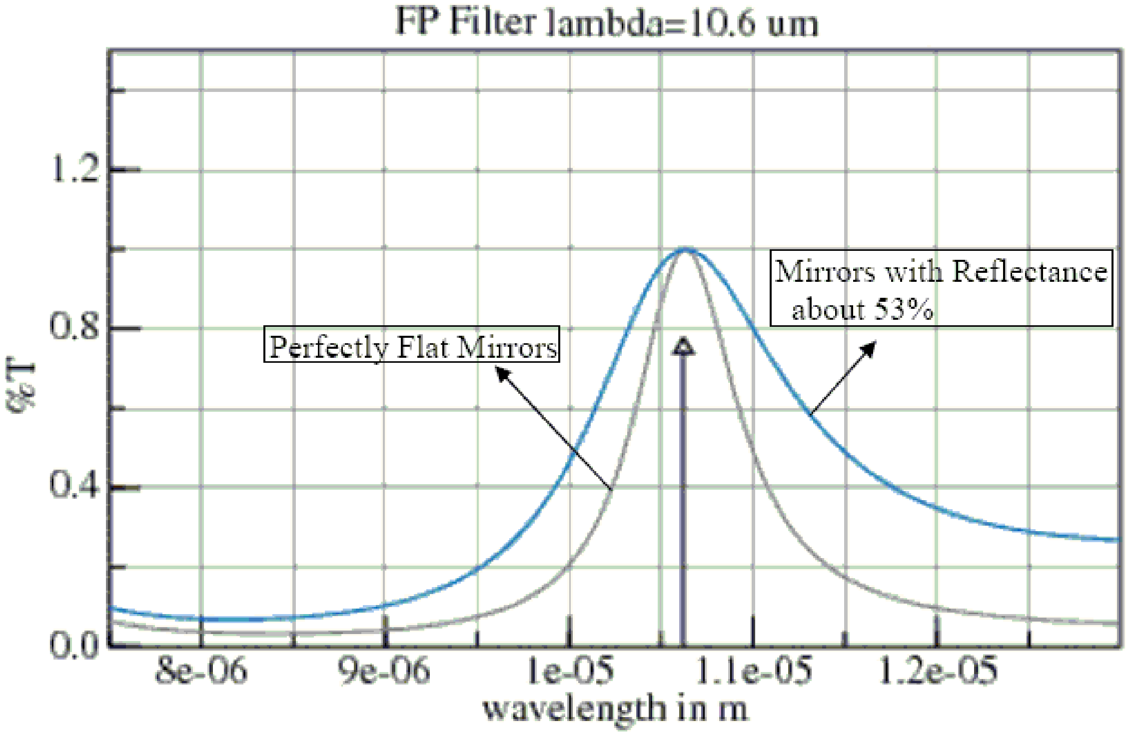

Figure 8.19: A comparaison between the result of FP with perfectly flat mirrors and non-ideal mirrors that result in reflectance of 53%.

The actual spectrum of the 10.6 μm wavelength is more related to a reflectance of approximately 53% which corresponds to a finesse of 4.86. The reduced finesse is mainly due to the surface roughness which can have been accured during the fabrication process specifically during the Si etching process [75,76].

CHAPTER IX: CONCLUSION

In this work we demontrated the possibility of fabricating a tunable optical filter based on Fabry-Perot interferometer, using ZnO and Ge as the mirrors dielectric materials.

The filter was designed to work in the mid-infrared spectroscopy applications. One important application for such filter will be in the wavelength range between 8 μm and 10 μm which target the infrared signature of glucose molecule.
This will, potentially, allow us to measure the glucose level in the blood without the need of pricking one's finger.

There are, however, some concerns associated with spectroscopy that we need to further study. These concerns are outlined below.

1- Molecules Interferences

There are many molecules circulating in the bloodstream and each has its own IR signature, we don't know how many of these molecules may possibly cause an interference with measuring the glucose signal.

2- Infrared Light Penetration depth

The IR light in the mid-infrared region tends to have a short penetration depth. That is the light doesn't not penetrate too deep in the skin. One way to mitigate this problem will be to measure the reflected light as opposed to the transmitted light, or may be use an implantable device that is replaceable after certain period of time.

REFERENCES

[1]. Kwok Leung Ong, Bernard M.Y. Cheung, Louisa Y.F. Wong, Nelson M.S. Wat, Kathryn C.B. Tan and Karen S.L. Lam. *Prevalence, Treatment, and Control of Diagnosed Diabetes in the U.S. National Health and Nutrition Examination Survey 1999–2004*. Annals of Epidemiology, Volume 18, Issue 3, March 2008, Pages 222-229

[2]. diabetes.http://www.diabetes.org.[online] 2012.[Cited: March 3, 2012]. http://www.diabetes.org/diabetes-statistics.jsp

[3]. Centers for Disease Control. http://www.cdc.gov.[online] 2012.[Cited: March 3, 2012]. http://www.cdc.gov/diabetes/pubs/pdf/ndfs_2011.pdf

[4]. Arnold Henry Kadish and David A. Hall. *A New Method for the Continuous Monitoring of Blood Glucose by Measurement of Dissolved Oxygen.* Clin. Chem., Sep 1965; 11: 869 - 875.

[5]. John C. Pickup, Faeiza Hussain, Nicholas D. Evans, Olaf J. Rolinski and David J.S. Birch. *Fluorescence-based glucose sensors*. Biosensors and Bioelectronics, Volume 20, Issue 12, 15 June 2005, Pages 2555-2565.

[6]. John C. Pickup, Faeiza Hussain, Nicholas D. Evans and Nabihah Sachedina. *In vivo glucose monitoring: the clinical reality and the promise*. Biosensors and Bioelectronics, Volume 20, Issue 10, 15 April 2005, Pages 1897-1902

[7].Do-Hyun Kim; Ilev, I.K.; Kang, J.U.; *Using Mid-Infrared Glucose Absorption Peak Changes for High-Precision Glucose Detection*. Lasers and Electro-Optics Society, 2007. LEOS 2007. The 20th Annual Meeting of the IEEE 21-25 Oct. 2007 Page(s):226 – 227

[8]. Centers for Disease Control. http://www.cdc.gov.[online] 2012.[Cited: March 3, 2012]. http://www.cdc.gov/media/releases/2011/p0126_diabetes.html

[9]. International Diabetes Federation. http://www.idf.org.[online] 2012.[Cited: March 3, 2012]. http://www.idf.org/diabetes-evidence-demands-real-action-un-summit-non-communicable-diseases

[10]. Pickup J, McCartney L, Rolinski O, Birch D. *In vivo glucose sensing for diabetes management: progress towards non-invasive monitoring*. BMJ 1999, 319: 1289

[11]. Anke Sieg, Richard H. Guy, and M. Begon˜ a Delgado-Charro. *Noninvasive Glucose Monitoring by Reverse Iontophoresis in Vivo: Application of the Internal Standard Concept.* Clinical Chemistry 1383–1390 (2004)

[12]. Seoul National University .http://en.snu.ac.kr[online] 2012.[Cited: March 3, 2012]. http://melab.snu.ac.kr/melab/doku.php?id=research:research.in.melab:biosensor

[13]. Marco Ferrari ,Valentina Quaresima, Martin Wolf. *Progress of near-infrared spectroscopy and topography for brain and muscle clinical applications.* Journal of Biomedical Optics 12_6_, 062104 _November/December 2007_

[14]. Hilde A. Rinia, Mischa Bonn, Erik M. Vartiainen, Chris B. Schaffer, Michiel Müller. *Spectroscopic analysis of the oxygenation state of hemoglobin using coherent anti-Stokes Raman scattering.*

[15]. World of Molecules.http://www.worldofmolecules.com[online] 2012.[Cited: March 3, 2012]. http://www.worldofmolecules.com/foods/glucose.htm

[16]. anne keckler.http://www.annekeckler.com[online] 2012.[Cited: March 3, 2012]. http://www.annekeckler.com/wp-content/uploads/2008/03/glucose-molecule.gif

[17]. pre-diabetes.http://www.pre-diabetes.com[online] 2012.[Cited: March 3, 2012]. http://www.pre-diabetes.com/medical/definition-insulin.html

[18]. Harvard Men's Health Watch Volume 15 ,Number 6 January 2011

[19] Frank K. Tittel, Dirk Richter, and Alan Fried "Mid-Infrared Laser Applications in Spectroscopy"

[20] C.-P. Sherman Hsu, Ph.D. "Infrared Spectroscopy", Handbook of Instrumental Techniques for Analytical Chemistry.

[21] Case study by Robert R. Gotwals, Senior Computational Science Educator, the Shodor Center for Computational Science Education "Visualizing the Vibrations of Water"

[22] Eric V. Anslyn, Dennis A. Dougherty "Modern physical organic chemistry"

[23] Tridib Tripathy, B. R. De, "Making Sense About Dipole Moments" Journal of Physical Sciences, Vol. 12, 2008, 155-172 155

[24] Jasco. "Fourier Transform Infrared (FT-IR) Spectroscopy, Theory and Applications" [online] 2012 [cited:January 29,2012] www.jasco.hu/konyvtar/FTIR-Presentazione.PPT

[25] Peter Signell "*continuous spectra: planck's law*". Michigan State University

[26] J. S. Tenn "*Planck's Derivation of the Energy Density of Blackbody Radiation*" Sonoma State University

[27] Duncan Lawson. *The Blackbody Fraction, Infinite Series and Spreadsheets*. Int. J. Engng Ed. Vol. 20, No. 6, pp. 984±990, 2004.

[28] Ph. M. Kanarev .*The Law of the radiation of the perfect blackbody is the law of classical physics*. Journal of Theoretics Vol.4-2.

[29] G.W. Ewing. *Analytical instrumentation handbook, second edition*. Marcel Dekker Inc, New York; 1997.

[30] William L. Wolfe. *Introduction to radiometry.* SPIE Tutorial Texts in Optical Engineering Vol. TT29

[31] W. Konz, J. Hildenbrand, M. Bauersfeld, S. Hartwig, A. Lambrecht, V. Lehmann, J. Wöllenstein. *Micromachined IR-source with excellent blackbody like behaviour*.

[32] tadeusz piotrowski1, daniel tomaszewski, maciej węgrzecki, vladimir k. malyutenko, andrew m. tykhonov. *Planar silicon structure in application to the modulation of infrared radiation.* Optica Applicata, Vol. XLI, No. 2, 2011

[33]. Jasco. “Fourier Transform Infrared (FT-IR) Spectroscopy, Theory and Applications” [online] 2012 [cited:January 29,2012] www.jasco.hu/konyvtar/FTIR-Presentazione.PPT

[34] S.O. Kasap "Optoelectronics and Photonics: Principles and Practices" 294-2001.

[35] B. Van Zeghbroeck “ Principles of Semiconductor Devices” 2011.

[36] John G. Webster “The measurement, instrumentation, and sensors handbook” 1999.

[37] David A. B. Miller “Optical Physics of Quantum Wells”

[38] Conny Hansson, Krishna Kishore Rachavula “Comparative Study Of Infrared Photodetectors Based On Quantum Wells (Qwips) And Quantum Dots (Qdips)” IDE0626,Technical Report,IDE2006.

[39] Farhan Rana “Semiconductor Optoelectronics” Cornell University.

[40] B.R. Nag “Physics of Quantum Well Devices” 2001

[41] A. Goldberg, T. Fischer, S. Kennerly, S. Wang, M. Sundaram, P. Uppal, M. Winn, G. Milne, M. Stevens, “Dual-Band Imaging of Military Targets Using a QWIP Focal Plane Array”

[42] Wayne S. Holland, William D. Duncan, Matt Griffin “Bolometers for submm/mm-wave astronomy”

[43] Henrik Jakobsen, Christian Vieider, Frank Niklaus “MEMS-Based Uncooled Infrared Bolometer Arrays – A Review”

[44] S. Skchez , M. Elwenspoek, C. Gui, M.J.M.E. de Nivelle, R. de Vries P.A.J. de Korte, M.P. Bruijn,J .J. Wijnbergen,W . Michalke, E. SteinbeiS, T. Heidenblut, B. Schwierzi “A High-Tc Superconductor Bolometer On A Silicon Nitride Membrane”

[45] John C. Mather “Bolometer noise : nonequilibrium theory”

[46] Robert B. Bass “Hot-Electron Bolometer Fabrication”

[47] George Rieke “Bolometers, and other thermal detectors”

[48] Volkmar Norkus,Gerald Gerlach, “Process Technologies for High-Resolution Infrared Detectors
based on LiTaO3” DIAS Infrared GmbH . Publications . No. 11

[49] Bradley D. Fahlman “Materials Chemistry”. 2nd edition

[50] John D. Clayto “Nonlinear Mechanics of Crystals”

[51] Sidney B. Lan “Pyroelectricity: From Ancient Curiosity to Modern Imaging Tool”, 2005 American Institute of Physics, S-0031-9228-0508-010

[52] J. Vaughan, “The Fabry-Perot Interferometer: History, Theory, Practice and Applications”. Philadelphia: Adam Hilger, 1989.

[53] Naseem Rangwala , T. B. Williams , Chris Pietraszewski , Charles L. Joseph . “An Imaging Fabry-Perot System for the Robert Stobie Spectrograph on the Southern African Large Telescope”. Rutgers Astrophysics Preprint # 474

[54] M. Bartek, J. H. Correia and R. F. Wolffenbuttel. “Micromachined Fabry-Perot Optical Filters”. Delft University of Technology, ITS/Et, Laboratory for Electronic Instrumentation/DIMES, Mekelweg 4, 2628 CD Delft, The Netherlands

[55] S.O. Kasap "Optoelectronics and Photonics: Principles and Practices" 294-2001.

[56] Alastair P. Hibbins,a Matthew J. Lockyear, and J. Roy Sambles, “The resonant electromagnetic fields of an array of metallic slits acting as Fabry-Perot cavities”. JOURNAL OF APPLIED PHYSICS 99, 124903 (2006).

[57] N. Neumann, M. Ebermann,. Kurth, K. Hiller, S, “Tunable infrared detector with integrated micromachined Fabry-Perot filter”, J.Micro/Nanolith. MEMS MOEMS 7(2), 021004-01 - 021004-9 (2008).

[58] H. A. Macleod, “Thin Film Optical Filters”, 3rd Edition, Institute of Physics, London, 2001.

[59] Harold E. Bennett, “Reflectance, Scattering, and the Anomalous Skin Effect” in Encyclopedia of Optical Engineering, Volume 3, R. G. Driggers, Ed. New York: Marcel Dekker, 2003, pp. 2349–2357, invited book chapter.

[60] http://refractiveindex.info/?group=METALS&material=Aluminium

[61] M. Bartek, I. Novotný, J.H. Correia, V. Tvarożek “Quality Factor of Thin-Film Fabry-Perot Resonators: Dependence on Interface Roughness”.

[62] E.Jesper Eklund and Andrei M. Shkel. “Performance Tradeoffs in MEMS Sensors with High-Finesse Fabry-Perot Interferometry Detection”.

[63] G. A. Gary, E. A. West, D. Rees, J. A. McKay, M. Zukic, and P. Herman, “Solar CIV vacuum-ultraviolet Fabry-Perot interferometers”

[64] C. Amra, P. Roche, and E. Pelletier, “Interface roughness cross-correlation laws deduced from scattering diagram measurements on optical multilayers: effect of the material grain size” Vol. 4, No. 7/July 1987/J. Opt. Soc. Am. B.

[65] W. Cao, C. Denker, H. Wang, J. Ma, M. Qu, J. Wang, and P. R. Goode, “Characteristic evaluation of a near-infrared Fabry-Perot Filter for the InfraRed Imaging Magnetograph (IRIM)”.

[66] Carsten Denker, Alexandra Tritschler, “Measuring and Maintaining the Plate Parallelism of Fabry-P´erot Etalons”.

[67] Christopher M. Gittins and William J. Marinelli, “LWIR Multispectral Imaging Chemical Sensor”

[68] G. Allen Gary, K. S. Balasubramaniam, and Michael Sigwarth, “Multiple Etalon Systems for the Advanced Technology Solar Telescope”

[69] Joseph F. Mulligan, “Who were Fabry and Pe´rot?” 1998 American Association of Physics Teachers

[70] Małgorzata Je□drzejewska-Szczerska, Bogdan B. Kosmowski, Ryszard Hypszer, “The optimal construction of a fiber-optic Fabry-Perot interferometer”, PHOTONICS LETTERS OF POLAND, VOL. 1 (2), 61-63 (2009)

[71] V. G. Kohn, Yu. V. Shvydko , and E. Gerdau, “On the Theory of an X-Ray Fabry-Perot Interferometer”, phys. stat. sol. 221, 597 □2000)

[72] Chitanu Elena, Ionita Gheorghe, “Obtaining thin layers of ZnO with magnetron sputtering method”

[73] M. Suchea,S. Christoulakis, K. Moschovis1, N. Katsarakis and G. Kiriakidis, “nanostructured zno and zao transparent thin films by sputtering–surface characterization”.

[74] Jae Bin Lee, Hyeong Joon Kimb, Soo Gil Kimc, Cheol Seong Hwang, Seong-Hyeon Hong, Young Hwa Shinc, Neung Hun Lee, “Deposition of ZnO thin films by magnetron sputtering for a film bulk acoustic resonator”.

[75] E. D. Palik, O. J. Glembocki, I. Heard, P. S. Burno, and L. Tenerz, “Etching roughness for (100) silicon surfaces in aqueous KOH”, J. Appl. Phys. 70, 3291 (1991); doi: 10.1063/1.349263.

[76] Gregory t. a. Kovacs, Nadim i. Maluf, and Kurt e. Petersen, “Bulk Micromachining of Silicon”.

[77] Bettina Voutou, Eleni-Chrysanthi Stefanaki, “Electron Microscopy:The Basics”

[78] Bob Hafner, “Scanning Electron Microscopy Primer”

[79] A. Bogner, P.-H. Jouneau, G. Thollet, D. Basset, C. Gauthier, “A history of scanning electron microscopy developments: Towards ‘‘wet-STEM’’ imaging”

[80] Joseph D. Geller, “Magnification Standards for SEM, Light, or Scanning Probe Microscopy”

[81] Müllerová,L. Frank, “Very Low Energy Scanning Electron Microscopy”

[82] William R. Herguth, “Applications of Scanning Electron Microscopy and Energy Dispersive Spectroscopy (SEM/EDS) To Practical Tribology Problems”

[83]. Thermo Scientific. Introduction to Fourier Transform Infrared Spectrometry. www.thermoscientific.com [online] 2012. [Cited: February 5, 2012]. https://www.thermo.com/eThermo/CMA/PDFs/Various/File_52263.pdf

[84]. Sheffield Hallam University. Infrared Absorption Spectroscopy - Instrumentation www.shu.ac.uk [online] 2012. [Cited: February 5, 2012]. http://teaching.shu.ac.uk/hwb/chemistry/tutorials/molspec/irspec3.htm

[85] William Blake Martin, Sergey Mirov, Ramakrishna Venugopalan “Using two discrete frequencies within the middle infrared to quantitatively determine glucose in serum.” Journal of Biomedical Optics 7(4), 613–617 (October 2002)

[86] Business Insight, “The Diabetes Device Market Outlook to 2016 Epidemiology, market forecasts, new innovations, company profiles, and market developments” BI00043-001, March 2011

[87] Eye Sense. Product Concept. www.eyesense.com [online] 2012. [Cited: March 3, 2012]. http://www.eyesense.com/en/konzept.htm

[88] freedom meditech. Overview. www.freedom-meditech.com [online] 2012. [Cited: March 3, 2012]. http://www.freedom-meditech.com/index.php?submenu= Overview&src=gendocs&ref=About%20Us%20-%20Overview&category=About%20Us

[89] calisto medical. Technology. www.calistomedical.com [online] 2012. [Cited: March 3, 2012]. http://www.calistomedical.com/?cat=27

[90] Dira med. www.diramed.com [online] 2012. [Cited: March 3, 2012]. http://www.diramed.com/index.html

[91] Integrity applications. Product description. www.integrity-app.com [online] 2012. [Cited: March 3, 2012]. http://www.integrity-app.com/description.html

[92] Glumetrics. Glucath. www.glumetrics.com [online] 2012. [Cited: March 3, 2012]. http://www.glumetrics.com/product/glucath/

[93] Veralight. Scout DS. www.veralight.com [online] 2012. [Cited: March 3, 2012]. http://www.veralight.com/products_5.html

[94] Andrea Tura, “Advances in the development of devices for noninvasive glycemia monitoring: who will win the race?”, Nutritional Therapy & Metabolism 2010; 28 (1): 33-39.

[95] Scott E. Van Bramer “An Introduction to Mass Spectrometry” Copyright 1997

[96] The Hebrew University of Jerusalem. www.huji.ac.il. [online] 2012. [Cited: March 3, 2012]. http://chem.ch.huji.ac.il/nmr/whatisnmr/whatisnmr.html

[97] Michigan State University. http://www.msu.edu.[online] 2012. [Cited: March 3, 2012]. http://www2.chemistry.msu.du/faculty/reusch/virttxtjml/spectrpy/uv-vis/uvspec.htm

[98]Michigan State University. http://www.msu.edu.[online] 2012. [Cited: March 3, 2012].http://www2.chemistry.msu.edu/faculty/reusch/VirtTxtJml/Spectrpy/nmr/nmr1.htm

[99] Donald L. Pavia, Gary M. Lampman, George S. Kriz,James a. Vyvyan "Introduction to Spectroscopy", 4th Edition. 2009.

[100] Massachusetts Institute of Technology. http://www.MIT.edu.[online] 2012. [Cited: March 3, 2012]. http://web.mit.edu/spectroscopy/history/history-modern.html

[101] Michigan State University. http://www.msu.edu.[online] 2012. [Cited: March 3, 2012]. http://www2.chemistry.msu.edu/faculty/reusch/VirtTxtJml/Spectrpy/MassSpec/masspec1.htm#ms1

[102] Benjamin B. Dingel, Achyut Dutta "Photonic add-drop multiplexing perspective for next generation optical networks"

[103] Volker Quetschke "LIGO - Coherent optical length measurement with 10-18 m accuracy", 14th Coherent Laser Radar Conference.

[104] National Institute of Science Education and Research, http://www.niser.ac.in [online] 2012. [Cited: March 3, 2012]. http://niser.ac.in/~sanjay/teaching/PL/ZEEMAN_user.pdf

[105] Jae Won Hahn, Seung Nam Park, Chunghi Rhee "Fabry-Perot wavemeter for shot-by-shot analysis of pulsed lasers"